DEVELOPMENT OF AN UNMANNED AERIAL VEHICLE AND IMAGE PROCESSING TECHNIQUES FOR AGRICULTURAL APPLICATIONS

By

WILLIAM WADE YOUNG

Bachelor of Science in Biosystems Engineering

Oklahoma State University

Stillwater, Oklahoma

2020

Submitted to the Faculty of the
Graduate College of the
Oklahoma State University
in partial fulfillment of
the requirements for
the Degree of
MASTER OF SCIENCE
May, 2022

DEVELOPMENT OF AN UNMANNED AERIAL VEHICLE AND IMAGE PROCESSING TECHNIQUES FOR AGRICULTURAL APPLICATIONS

Thesis Approved:

Dr. Ning Wang

Thesis Adviser

Dr. John Long

Dr. Paul Weckler

ACKNOWLEDGEMENTS

Many people have influenced my ability to complete this Thesis and degree program, the sacrifices of which have not gone unnoticed.

I would like to first thank Dr. Wang for her tireless effort to expand my education and provide resources, as well as answering countless hours of questions. Entering graduate school during the COVID-19 pandemic was uncertain for everyone, but you made sure things felt normal. Dr. Wang, your efforts- for all students- are admirable.

I would like to thank Dr. Long and Dr. Weckler for their continuous support and effort. Through teaching additional courses, fielding random questions, and giving expert advice, your assistance was very much appreciated. This committee was an unlimited source of knowledge, and for that I am extremely grateful.

In addition, I would like to acknowledge my colleague, road trip partner, and friend, Austin Pickering. Countless hours on the road, in the field, and oftentimes lost, I was always grateful to have company. Though we challenged each other continuously, I greatly enjoyed our time together. I wish you the best in your career.

I would like to thank my parents for their steadfast support and counselling. Though you may often have been confused by the things I was saying, your attentiveness and compassion were constant and reliable. Thank you both for your sacrifice, attentiveness, and helpfulness.

Finally, I would like to thank Taylor Holmquest. Your consistency, patience, and understanding were always appreciated. You pushed me when I needed to be pushed, and you pulled me away when I needed a break. Though you may not have understood everything I told you, you constantly tried to keep up and provide thoughtful insights. Your helpfulness and reliability are two things that I admire the most. I could not have done it without you, thank you.

Name: WILLIAM WADE YOUNG

Date of Degree: MAY, 2022

Title of Study: DEVELOPMENT OF AN UNMANNED AERIAL VEHICLE AND IMAGE PROCESSING TECHNIQUES FOR AGRICULTURAL APPLICATIONS

Major Field: BIOSYSTEMS ENGINEERING

Abstract: In this study, an unmanned aerial vehicle (UAV) was built for use in small breeding plots. The UAV was constructed from readily available off-the-shelf components, such as the Cube Orange flight controller and HERE3 GPS. The UAV was a hexarotor design powered with a 4s 9000mAh battery. The UAV underwent a series of tests across multiple dates to determine flight path accuracy. Two flight heights (30.48m and 60.96m) were taken on multiple dates. A custom pan tilt servo gimbal was constructed capable of carrying multiple cameras in different configurations. The gimbal was tested using a series of different weights and mounting locations. A case study was completed to demonstrate usefulness of the system and the open-source image processing pipeline which can be used with images captured from the custom built UAVs. In testing, the average lateral error of the UAV was 0.2m. The average vertical errors were 0.06m, and 0.33m according to the data with the extended Kalman filter (EKF) and the built-in barometer, respectively. The average errors of the gimbal at maximum load was 1.2 degrees in the pitch direction and 1.7 degrees in the roll direction. The case study demonstrated that free, open-source software can be successfully used to process images from the UAV system.

TABLE OF CONTENTS

LIST OF TABLES

Table Page

LIST OF FIGURES

Figure Page

Figure Page

CHAPTER I

INTRODUCTION

1.1 Overview

The future of agriculture relies on the thoughtful uses of new technologies and a willingness to apply and adapt to these technologies. Tools such as yield monitors, guidance systems, soil maps, and variable rate application systems are now widely used on many farms. In 2010, for instance, yield monitors were found to be used on 70% of all corn cropland (Schimmelpfennig, 2016). Combined with high-accuracy real-time-kinematic (RTK) Global Positioning Systems (GPS), these tools can be used to increase producer's output. Precision Agriculture can be defined as the use of the aforementioned technologies (among countless others) to capture high-resolution spatial and temporal data to further the efficiency and output of farming practices. Combined with the rise of the "Internet of Things" (IoT), farmers are able to use data captured through precision agriculture techniques to understand them in a better manner. Things such as yield maps may be processed online and displayed to monitors, allowing operators to view field conditions in real time.

1.2 Remote Sensing and UAVs in Agriculture

While much of agriculture relies on qualitative data and observations, precision agriculture has made it possible to use data-driven decisions to increase yield. Remote sensing has risen to become an important aspect of precision agriculture. Remote sensing is the use of non-destructive methods of data collection where a sensor does not physically touch or interact with the subjects. Remote sensing comes in many forms, but the most common applications in agriculture rely on cameras and multi-spectral sensors. These sensors are capable of capturing signals at different wavelengths of light, the most common being visible light (Red, Green, Blue), Near-Infrared and Infrared light (Wójtowicz, Wójtowicz, & Piekarczyk, 2016). In the past, remote sensing relied on satellites and manned aircraft. While these technologies are useful in large areas, they oftentimes lack spatial resolution. Furthermore, their temporal resolutions may lack due to orbital paths if using satellite imagery, operator availability, cost, and/or other factors associated with manned flight.

With the above listed issues found with the satellite- and manned aircraft-based remote sensing, Unmanned Air Systems (UAS) have become increasingly used in agriculture. Globally, the agricultural UAV market is expected to reach a $4.4 Billion valuation by 2024 (GIA 2021.) This valuation has been caused by the rise of consumer-grade UAVs often used for filmmaking, racing, and other leisure. With the decreased complications of flight (autopilots and position hold functions), high resolution cameras (mostly RGB), and increased flight times associated with consumer grade drones, their adoption to agriculture is to be expected.

With increased agility and flight time, UAVs can be flown at lower altitudes in a crossing pattern (defined as a “mapping mission”) to capture a multitude of geotagged images with high overlap. Many applications exist to provide fully autonomous mapping missions (many including takeoff and landing) relying on high-accuracy GPS systems. Other products exist to take these

geotagged images and “stitch” them into orthomosaic photos. These allow for a high spatial resolution (1-10cm) without the use of ultra-high resolution images. Using Global Information Systems (GIS), these orthomosaics can be used for many different types of analysis, both qualitative and quantitative.

1.3 Applications and Use Cases of Agricultural UAV

Agricultural engineering research is a unique field, in that research duties overlap heavily between agronomic-based research (such as plant physiology, crop and soil evaluation, etc.) and engineering-based research focusing on mechanical, electrical, and software components. There has been a need established in the department of Biosystems and Agricultural Engineering at Oklahoma State University for a UAV to carry different sensor payloads to assist in data collection in multiple agronomic projects. This UAV will perform field mapping and collect remote measurements in various research plots.

As previously mentioned, satellites and manned aircraft have long been used in remote sensing applications, but are not capable of high spatial resolution, especially in small breeding plots encountered in agronomic research. Other techniques include manual data collection (carrying sensors such as spectrometers) and ground-based rover systems carrying different payloads. Ground-based rover systems are faster than manual measurements, but lack the ability to gather data on an entire field in a reasonable amount of time. For these reasons, it was determined a UAV would be needed.

Because of numerous frame types, manufacturers, and models of UAVs available on the market, a search was conducted to determine if there were any suitable models available on the market. The following list builds an initial framework for deciding on a product. These are the five most important factors associated with the desired UAV, based on targeted functionality.

1) Payload

The UAV must be configurable to many different sensor payloads such as RGB and multispectral cameras, LiDAR, and other remote sensing technologies. To provide ample lifting capacity for different sensors, the UAV should be capable of lifting a payload of up to 1kg.

2) Flight Time

Flight time of a UAV is associated with the all-up-weight (AUW) of the vehicle and payload, and the capacity of the battery. Because the primary use case of this UAV will be field mapping, a longer flight time allows a larger area to be covered in a single flight. For the purposes of this study and future studies on research plots, 10 minutes will be used as the target flight time to 20% battery power (to account for landing time.)

3) Ease of operation

Operating a UAV in a field should not be a complicated task, so ease of operation was considered in the search for a UAV. Useability applies for both the applications used to create flight paths and monitor the UAV in flight as well as stability and responsiveness of the UAV in flight (such as GPS or visual based location holding.)

4) Price

Some UAVs can be prohibitively expensive. For the purposes of this study, a budget of $2,000 was established.

5) Configurability

The UAV must be easily configurable to be able to work on numerous future projects, and must have software capabilities that allow the addition of extra sensors and devices.

After a thorough search, it was determined that most of the UAVs available on the market were too costly. Many of the major UAV manufacturers also have software which is proprietary and not easily able to be manipulated. With the rise of open-source alternatives to many of the name brand manufacturers of UAVs, it was decided that a custom UAV would need to be constructed to meet the above requirements of the study.

1.4 Objectives

The overall objective of this project is to develop a custom-built UAV platform to be used in agronomic research and develop a framework for image processing which may be used as a starting point for future research and development. Many processes will be investigated after the construction of the UAV to evaluate its uses, functionality, and practicality. The objectives are listed below:

1) Design and test a UAV platform
2) Design and test a sensor mounting solution
3) Develop a pipeline for processing data captured from the UAV platform
4) Demonstrate the platform's functionality in a case study

The deliverables of this project should be a functional and ready-to-fly UAV platform, a ground control station, a re-configurable sensor mounting solution, and a pipeline of methods for image processing.

CHAPTER II

LITERATURE REVIEW

The literature review below highlights important areas of interest pertaining to this project and analyzes previously used techniques that can be used to aid in the design of this study. Four main categories were reviewed: UAVs in Agriculture, Remote Sensing Techniques and Applications in Agriculture, and Cotton Maturity. Each of these sections consists of subsections that are particularly related to this study.

2.1 UAVs in Agriculture

While Unmanned Aerial Vehicle is the technical name for remotely operated aerial vehicles, the name “drone” has become popular to recognize these devices. The development of UAVs can be traced back to World War I, but lacked stability and controllability in this time period (Keane & Carr, 2013). Advances in the 1950’s utilized UAVs as “target drones”, while later in the Korean War UAVs were used for reconnaissance. UAVs began their move into agriculture as early as 1985, when Yamaha, Japan, introduced a programmable unmanned helicopter to gather aerial imagery (Billingsley et al., 1984). For many years, the UAVs used in agriculture were in the form of single prop helicopters and fixed wing aircraft (Herwitz et al., 2004).

In 2010, Parrot, a French company, introduced a UAV at the Consumer Electronics Show in Las Vegas, Nevada. This UAV was a multicopter with a 12-minute flight time and operated by a smartphone device. In 2013, a competitor, DJI from Shenzhen, China, released their Phantom 1 drone. The Phantom 1 was a multicopter with a 10-minute flight time carrying a GoPro camera to capture aerial imagery. In the years since, both companies have grown to be the leading options for agricultural UAVs by releasing designs which are capable of long flight times, ease of use, and large payloads to carry a multitude of sensors.

After the US Congress passed the Modernization and Reform Act in 2012 which allowed citizens to own and operate UAVs which weighed underneath 25kg, there was a large jump in attention to the remotely-piloted vehicle industry (Freeman & Freeland, 2015). Freeman (2015) evaluated article in newspapers between 2010 and 2014 to look at the public interests in UAVs. Between 2012 and 2013 the combination of the keyword “agriculture” and “unmanned” in publications jumped from 398 to 1117. In the years since, research related to UAV applications in agriculture have increased significantly. The future economic impact of UAVs in agriculture has various outlooks, but most estimate that the market will grow from ~ 1 billion USD in 2020 to over 5 billion USD by 2026 (Industry Arc, Markets and Markets 2021). These advances are driven by major companies’ development in the sector.

With the ease of use offered by many modern products, farmers and producers are able to deploy UAVs for a large range of uses. The most common uses are in crop scouting and analysis. In one study, a single rotor UAV was used to fly multiple sensors over a potato crop and accurately develop scouting maps for uses by producers. (JérômeThéau et al., 2020). In this study, the best sensors were selected based on physiological properties of the plants. The study focused on the sensors with red, green, near infrared (NIR), and thermal light bands to create orthomosaic images of the crop. The images were then processed to highlight locations of interest pertaining to disease, insect presence, and development problems. UAVs can also be useful in

weed scouting. In one project, a UAV was deployed with a 12-megapixel camera to gather images of a crop to identify and localize weeds between rows (Li et al., 2016). This project showed that with proper data processing methods, RGB-based UAV imagery could be used for generating weed infestation mapping. UAVs were also used in conjunction with Convolutional Neural Networks (CNNs) to determine presence of disease in vineyards at both the vine level and the leaf level with high accuracy (Kerkech et al., 2020). In this project, the authors used a UAV with a 20-minute flight time to capture RGB and NIR images with a resolution of 1cm/pixel. The high-resolution images were then used in different algorithms to provide useful data. UAVs have also previously been used in the detection of bacterial wilt in peanut crops by using red, green, NIR, and red-edge sensors (Chen et al., 2020). On top of disease detection, other types of crop stress factors have been identified with UAV-based systems, such as drought effects in soybeans (Zhou et al., 2020). Many of the above uses highlight UAVs as useful, high efficiency methods to gather remote sensing data related to crop metrics.

Several different configurations of Agricultural UAVs exist. The most common types are multicopters or fixed wings. Multicopters utilize several pairs of motors (most commonly 4 or 6 motors) to achieve stability. Fixed wings are formatted much like a traditional aircraft, with forward facing thrusters and props. In a survey of 100 papers related to UAV applications in agriculture, Tsouros (2019) noted that 72% of the studies used multicopters, while 22% utilized fixed wing platforms. The majority of works used a multicopter due to their slow flight speeds for low altitude imaging, ease of use, and maneuverability (Tsouros et al., 2019).

The frame configuration and arm design of a multicopter can also be vastly diverse. As previously mentioned, a multicopter generally relies on a pair of motors working in opposite rotations to achieve balance, and these pairs can be duplicated to provide stability. The most common configuration is that of a “quad-copter,” which utilizes four motors in an “X” configuration. Other common forms are 6 and 8 rotor configurations, which are often boasted as

more stable and reliable than a quadcopter due to their redundant motor configurations. Neimiec (2018) developed a reconfigurable UAV to compare the efficiencies and controllability of a quad-copter (4 props), hexa-copter (6 props), and octo-copter (8 props) configurations against a deca-copter (10 props). In this study, the maximum useful weight metric was used as a comparison factor among the designs. Maximum useful weight was defined as the difference between the maximum gross weight and the empty weight of the UAV, where the maximum gross weight was the sum of all motor-prop combinations thrust capabilities (Niemiec et al., 2018). In general, a larger useful weight required more motors to achieve the same lifting capabilities while also incurring losses. At 29% of the useful weight of the deca-copter, the quadcopter required 14.1% more power than a deca-copter, the hexa-copter required 4.7% more power, and the octocopter power required was relatively close to that of the deca-copter. At higher loads (75.4% of the deca-copter useful weight), the hexa-copter required 10.7% more power, and the octocopter required 3.7% more power. This power requirement was caused by the higher speeds required by each prop to spin when there were less props present on the design. The author stated that in their experiment (where maximum useful weight of the deca-copter was 4.7kg,) the hexa-copter was "power optimal" during hover operations in weight ranges between 0.25 and 0.75 kg. The authors did not specify if this weight included the battery. The hexa-copter demonstrated higher longitudinal position variance as opposed to the other designs, but had a similar latitudinal variance to the octocopter and deca-copter designs, which were much lower in comparison to the quadcopter. The study showed that a hexa-copter or octo-copter design was preferred, due to controllability and useful weight of the different designs.

In each frame design, the effects of motor mounting location (above or below the arm) are also of consideration. Theys et al. (2016) compared motor efficiency based on configurations of the arm in a "pusher" layout, a "puller" layout, two blade vs three blade props, arm design coaxial designs, and propeller overlap designs. Pusher configurations were laid out where the

propeller was mounted underneath the arm of the UAV, whereas in a puller layout the motor was mounted above the arm much like a traditional helicopter. While puller layouts were more common, the author determined that there is roughly a 3% increase in efficiency. In the 3-blade vs two-blade propeller experiment, the author noted a loss of 4% efficiency when using a three-blade propeller, but also noted a significant decrease in sound when using a 3-blade propeller. Three different arm designs were tested including a 25mm carbon fiber tube, a 10mm carbon fiber square tube, and a 3D printed nacelle. The thin 10mm square design performed the best in testing, while the 25mm carbon fiber tube performed the worst. The efficiency difference between the two was most nearly 4%. For the sake of simplicity, the proposed work will not consider a coaxial or overlapping propeller design.

2.2 Remote Sensing Applications in Agriculture

Remote sensing technologies generally rely on camera systems with light filtering lenses to capture signals at several bands of visible and NIR light, which can then be processed to provide different vegetative Indices. Wojtowicz (2016) states that the most useful spectral range of light for agricultural applications are visible light, infrared, and thermal Infrared. The combination of many bands of light by some equation is generally referred to as a vegetative index. The best vegetative indexes correlate heavily to some biological or physical parameter of the crops being measured.

Satellite-based systems have been used for over 50 years to determine crop characteristics (Zhang et al., 2020). The author introduced many different systems which are currently in orbit to capture high resolution visible and multispectral images. The spatial resolution of these systems ranges from 0.31m/pixel – 0.86 m/pixel. Most of the systems contain Red, Green, Blue, and Near-Infrared sensors. The temporal resolution of the systems ranges from 1-5 days.

Aerial based systems can provide a higher spatial resolution than satellite imagery, but come with the complications associated with mounting the sensors on the aircraft (Yang et al., 2014). Yang (2014) flew a manned aircraft with a custom camera array over cotton crops in Texas, USA, at an altitude of 1000-10000ft (~305m – 3050m). The altitudes provided spatial resolution of 0.1m – 1m per pixel. In vineyards, it was shown that an aircraft and satellite combination may be effective in highlighting features (Matese et al., 2015). This study compared the cost and effectiveness of satellite (5m resolution), aircraft based (0.5m resolution), and UAV based (0.05m resolution) to capture multispectral imagery. The combination of aircraft and satellite imagery provided useful information, but was considered much more costly than the UAV based system. The UAV based system was less costly on a smaller scale, showing that the application of remote sensing technologies should depend on the use case.

In recent years, there has been a shift towards using UAVs in place of manned aircraft for many remote sensing operations (Chen, 2020; Kerkech, 2020; Li, 2016). Chen (2020) compared ground-based hyperspectral data to data collected by a Parrot Sequoia Multispectral Camera (Parrot, Paris, France) containing red, green, blue, red edge, near-infrared bands on peanut plots in China to determine presence and severity of bacterial wilt. The authors compared physiological ground ratings to narrow band hyperspectral data to determine the bands of light which most closely follow the physical traits of the crop. The result showed that the UAV images were sufficient to identify bacterial wilt at field level. In cotton crops, UAVs have been used to collect remote sensing data to predict yield (Feng et al., 2020). A multi-sensor array consisting of a multispectral camera, RGB camera, and thermal camera were flown over cotton crops to determine yield potential of the field. Images were geo-aligned with yield monitor data from the harvester.

In agriculture, remote sensing data is usually focused on multispectral, hyperspectral, or infrared thermal data. Hyperspectral data is capable of gathering hundreds of different bands of light with very high resolution, oftentimes as low as 1-10nm (Feng et al., 2020). Multispectral cameras uses fewer bands, but are easier to configure into a payload that a UAV can carry. For agriculture, commonly used bands of light are red-edge (680nm-750nm) and NIR (750nm – 2500nm), because they are highly sensitive to changes in physical crop changes (Deng et al., 2018). Different cameras have different accuracy; therefore, ground calibration targets are necessary in any application of multispectral remote sensing. Thermal radiometric cameras can also be affixed to a UAV to capture the radiation from crop canopies. Thermal data can be used in crop water stress monitoring, disease detection, yield estimation, and phenotyping (Messina & Modica, 2020).

2.3 Image Processing Methods and Analysis

UAV imagery is generally used to create high-resolution geo-located orthomosaic images. These images are then used to identify exact locations of interest in a field. Advanced photogrammetry techniques available currently can provide high accuracy using RTK GPS data (Barry, et. al., n.d.). Commercial software such as Pix4Dmapper (Pix4D, Prilly, Switzerland) and Agisoft Photoscan (Agisoft, St. Petersburg, Russia) are available to create orthomosaic photos from a batch of low altitude, high-resolution photos. These software packages also allow for the addition of ground control points, which can make orthomosaic photos far more accurate. Open-source packages such as Open Drone Map are also available, but lack some advanced abilities associated with the aforementioned packages and may also take extra time to install.

2.4 Cotton Maturity Ratings and Defoliant Applications

As of 2020, Oklahoma is the fourth largest producer of cotton in the nation (Stotts, 2017). The harvest of cotton is a considerably difficult task, and producers have to take into account fiber quality as well as timing to ensure the best harvest. Harvest aids are generally applied to speed along the natural process of defoliation (Byrd, 2019). They are used to cause defoliation, open cotton bolls, and prevent regrowth. The application methods of harvest aids vary between seasons, fields, and locations. Generally, the application of harvest aids is based on the maturity of the cotton plant. Current methods of rating maturity include the Nodes Above Cracked Boll (NACB) method, percentage open boll, or the knife test. These methods are used to determine the timing of harvest aid applications, which should generally be during a 4-5 NACB, 60-70% percentage open boll, or finding a firm, difficult to slice through boll with the knife test. Incorrect timing of applications can result in lint loss, reduction in micronaire, and a loss of fiber weight (Boman, 2015).

CHAPTER III

DEVELOPMENT AND TESTING OF AN UNMANNED PLATFORM

3.1 Design Goals and Construction of a UAV Platform

After reviewing literatures related to the design of the UAV, a hexacopter frame type was selected which was more efficient for the load range chosen (up to 1 kg), as well as could provide some additional stability and redundancy in flight. The frame selected was a Tarot 690 Carbon Fiber hexacopter frame. This frame allowed for 10-13" propellers and had a weight of 600 grams, which was sufficient for the loads of small cameras and sensors for the desired outcomes of the proposed work. The frame also came with battery mounting bracket, as well as two parallel carbon fiber tubes which served as mounting brackets for sensors, gimbals, etc. Retractable landing gear were added to the frame so that the landing gear would not hinder the visibility of the cameras during heavy pitch and roll movements in flight. These landing gears were of carbon fiber construction and operated by two servo motors for automatic control by the flight controller.

The motors selected were matched to the frame and propeller sizes. As the propeller size was limited to 13", carbon fiber 1045 propellers were selected. The motors used were Lumenier 740kV motors, which had a maximum continuous current of 24 amps and a weight of 92 grams. As recommended by the motor's manufacturer, a 4s

battery and a 1045 propeller size were used. The motors had a manufacturer rated efficiency of 84%.

The battery selected for the UAV were 4s, 9000mAh, and 100C Lithium Polymer batteries purchased from Zeee (Zeee Power, Guangdong, China). At 4s, these batteries full-charge voltage was 16.8V. The electronic speed controllers (ESC's) chosen were HobbyWing Platinum Pro 30A ESCs (HobbyWing, Shenzhen, China). The 30-amp rating was important, as it nearly matched the motors chosen so that the motors could run at their maximum power if needed. Custom 3D printed covers were designed and created to cover the ESCs and protect from potential damages. To breakout power from the batteries to the ESC's and flight controller, a Matek power distribution unit (Matek Systems, China) was used. The power distribution unit had six pairs of positive and negative solder pads for six ESCs, an XT60 connector style, and battery elimination circuit (BEC) regulated 5V and 12V outputs. The 5V and 12V outputs were necessary for any additional components which would be mounted to the UAV, such as sensors, gimbals, and data acquisition devices.

For control of the UAV, a Cube Orange flight controller (ProfiCNC, Australia) with a standard ADS-B carrier board was used. The Cube Orange had a multitude of useful features, such as three temperature compensated redundant internal measurement units (IMU's), ADS-B functionality, a 32-bit ARM microcontroller, and an additional 32-bit failsafe co-processor (ardupilot.org). It contained two UAV-CAN ports, I2C functionality, five UART ports, SPI ports, multiple analog inputs, and 14 PWM outputs (four of which could be configured as relays via a ground control station). The flight controller was mounted on custom 3D printed brackets to the center of the UAV. A

HERE3 GNSS (ProfiCNC, Australia) was used as the only GPS unit on the UAV. The HERE3 utilized a u-blox M8N GNSS module, had RTK capabilities, and could be connected via UAV-CAN. The UAV-CAN protocol had a benefit over traditional UART GPS devices due to simplicity in wiring, which was critical in a UAV construction to increase robustness. The HERE3 data sheet specified an accuracy of 2.5m in 3D fix, and 0.025m in RTK. It also contained a built-in compass, a gyroscope, and an accelerometer. For best results, the GPS was mounted on a 158.75mm foldable mast. While the ground control station was able to calculate the offsets of the GPS mounting location in relation to the frame center of the UAV, the GPS was placed in the center front of the UAV. GPS mast placement was also useful in identifying heading visually during flight.

For the user-control of the UAV, a ground control station was used via a 3DR 915mHz SiK telemetry radios (3D Robotics, California, USA), as well as a traditional 2.4GHz handheld RC transmitter Radiolink AT-10 (RadioLink, China), which had eight toggle switches, three rotary switches, and two 2-axis joysticks, and a small display to show relevant data. The Radiolink AT-10 could transmit 10 channels of information, so not all switches were able to be used on independent channels; however, multiple switches could be applied to the same channel to change values. The receiver used was a Radiolink R12DS (RadioLink, China), which had PWM outputs as well as SBUS capabilities, which was the protocol the Cube Orange used for RC input (the Cube Orange could also use PPM, but this required an additional conversion device). There were many ground-control stations commercially available, but by far the most commonly used and supported was Mission Planner. Mission Planner was an application which could be installed on any computer with Windows, Macintosh, or Linux operating

systems. In this study, the computer used was a Dell Latitude 3390 2-in-1. The 915MHz, 500mW telemetry radios were installed on the UAV to a UART port, as well as plugged in via USB to the laptop. A pair of these radios provided a constant downlink of telemetry information from the UAV (namely position, status of outputs, battery voltage, etc.). These radios allowed for a longer-range communication than that of traditional 2.4GHz controllers. However, the longer range was not important to the scope of this study as a recreational or educational use of UAVs in the United States required the UAV to stay within visible distance. The RTK corrections for the GPS were also sent through the telemetry radios. The GPS base station used was an Emlid RS+ GPS unit (Emlid, China), which was connected to the ground control station on the laptop via a TCP interface. The RTK corrections were setup via Mission Planner. Figure 1 below shows a diagram of connection types between the ground control station and the UAV.

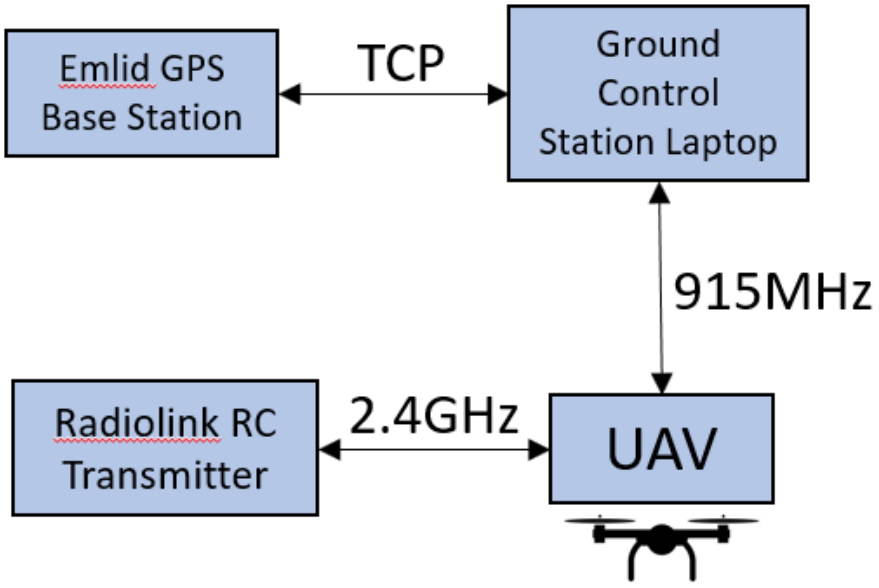

Figure 1. UAS system diagram

3.2 UAV Platform Test Criteria

The UAV platform under development had a targeted use in research plots. The primary functionality of this UAV would be flying pre-determined flight paths over a field and capturing images with the ability to create ortho-mosaics for future analysis, with a desired temporal resolution. Due to the focus being on pre-mapped missions and image analysis, flight control, stability, and vibrations were out of the scope. Flight path accuracy and flight time were far more important. Flight time dictated the coverage ability of the UAV in a single day. Flight path accuracy ensured that proper overlap and image coverage could be achieved, so later uses of the images collected could be more significant. Hence, the purpose of the experiments was to test the flight time and flight path accuracy of the developed UAV platform under an actual season-long study. Flight path accuracy was defined as two parameters, vertical error which was the difference in altitude between the planned flight path versus the achieved flight altitude and lateral error which was the difference in location along the flight path vs. the actual UAV location in the horizontal plane. Equations 1 and 2 show the calculations for the two errors in meters (m).

$$V_{error} = |Desired\ Altitude - Achieved\ Altitude| \quad (1)$$

$$Lateral_{error} = |Desired\ Lateral\ Location - Actual\ Lateral\ Location| \quad (2)$$

Battery life is of great importance with a UAV. Many commercial systems include “smart battery monitors” which can report a percentage charge to the user. Many mobile devices display percent charge, but this technology is challenging and expensive for custom built UAVs. Battery charge of a lithium polymer battery relied on battery voltage, therefore, the battery voltage was monitored during all flights. A charged lithium

polymer cell had a voltage of 4.2V, and a completely discharged battery would report a voltage of 3.2V. Because 4s batteries were used in this study, multiplying the max charge by the number of cells resulted in a full charge voltage of 16.8V, with 9000mAh of capacity. A fully discharged battery would report most nearly 12.8V. A LiPo battery is generally never discharged below 25% of its capacity (which is roughly 14.99 volts without load). Using Equation 3, the estimated voltage of the lithium polymer battery at 25% was calculated.

$$Voltage = (4.2 * number\ of\ cells) - \big((4.2 - 3.2) * number\ of\ cells\big) * \%\ Charge \qquad (3)$$

As a note, this equation was only an estimation. Every battery was different. The actual usable capacities of each battery should be thoroughly tested. By solving the above equation for 25% charge remaining (75% discharge), the discharged or "safe landing" voltage of the battery should be 13.8 volts total, or 3.45 volts per cell.

3.3 UAV Platform Testing Methods

To test the platform and criteria from Section 3.2, a set of experiment was conducted as a case study over cotton crop. The experiment was performed at Oklahoma State University Caddo Research Station in Ft. Cobb, Oklahoma. The field center was located at 548827.08E, 3889676.81N Zone 14N. An overlapping flight path was established over the region of interest, based on the cameras being used. Two different elevations were used, 30.48m (100ft) and 60.96m (200ft). The altitude was measured relative to the home location of the UAV. The flights were completed over a course of six different dates between the 10th of September, 2021, and 14th of October, 2021. The same

flight paths were used for all the six dates. The flight speed was a maximum of 2 m/s for both altitudes. Figure 2 and 3 show the flight paths taken.

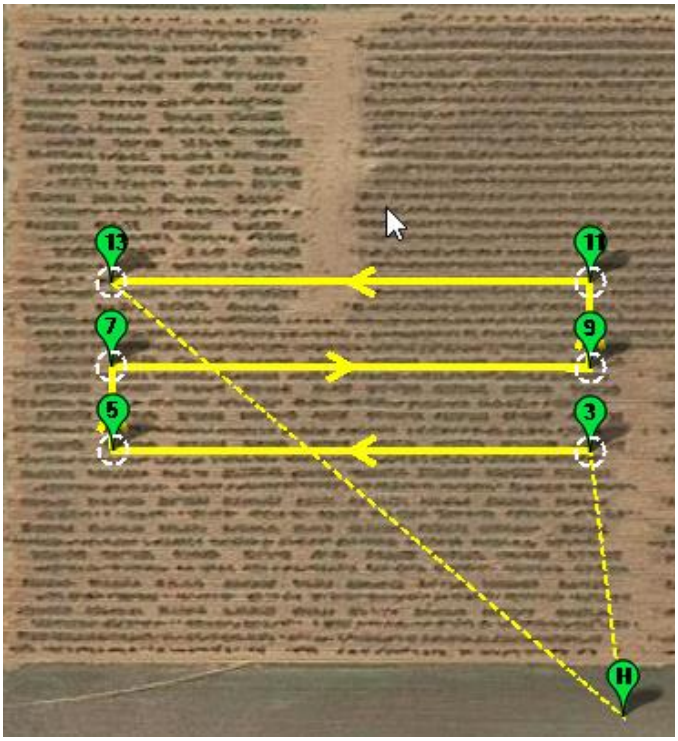

Figure 2. The flight path at an altitude of 30.48m

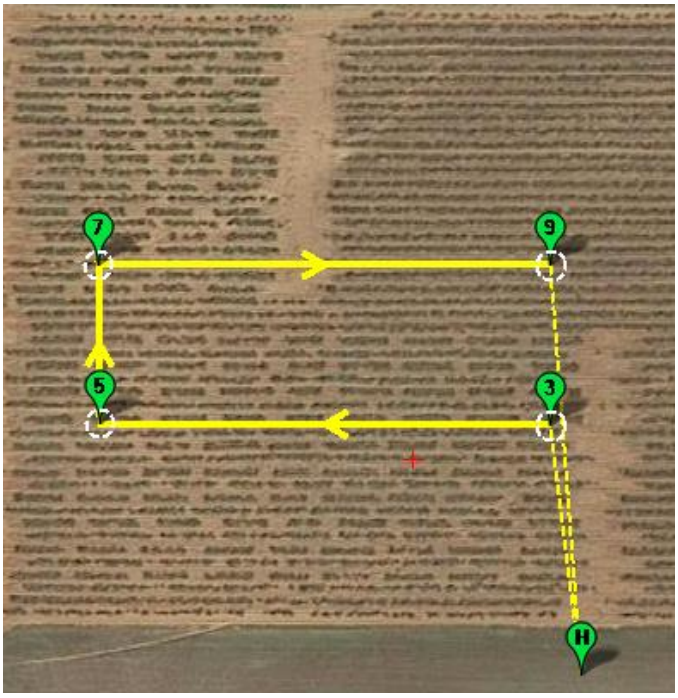

Figure 3. The flight path at an altitude of 60.96m

In all 12 flights, the UAV carried a payload of three cameras with a total weight of 202 grams (not including the gimbal). All flights began by placing the UAV on a landing board, starting the camera auto-shutter procedure, and taking off in auto-mode. The UAV followed the waypoint plan showed in Figures 2 and 3 and automatically landed at the end. The take-off and landing time, take-off and landing battery voltage, and thermal measurement of the black target background were collected and stored for each flight. Figure 4 shows the setup of landing zone and calibration targets for the UAV.

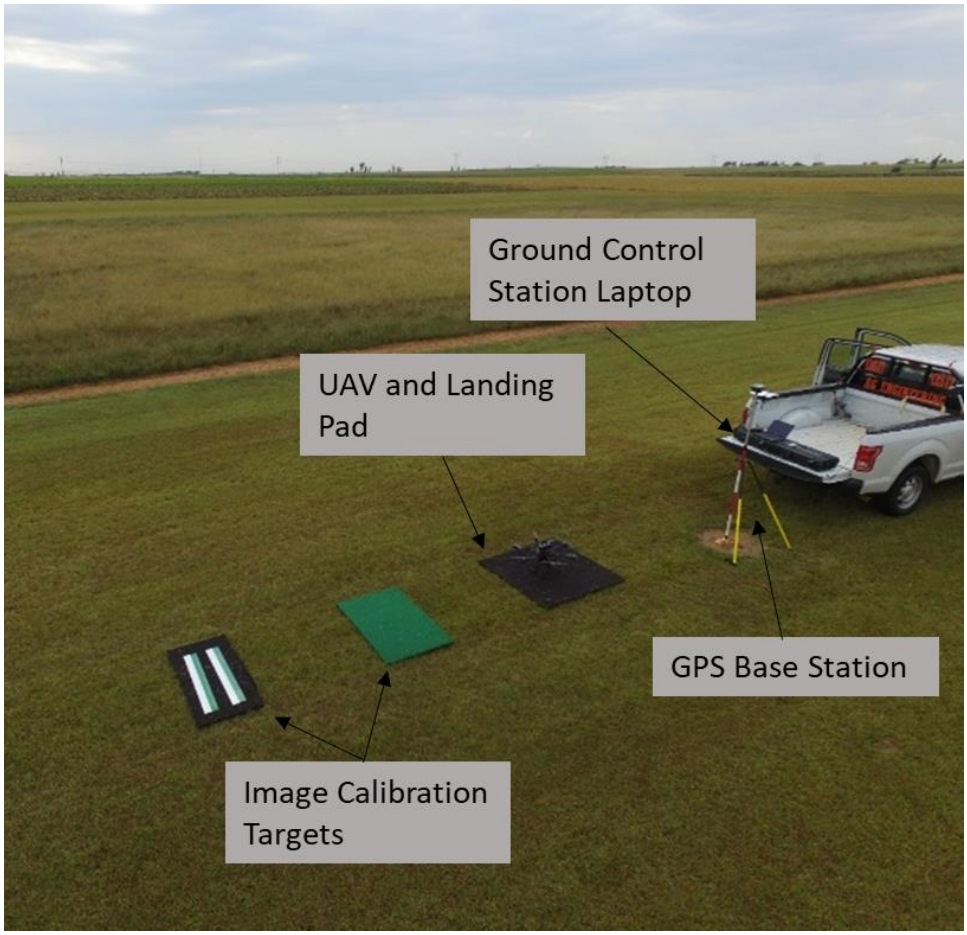

Figure 4. Landing zone and calibration targets

Prior to each flight, the RTK GPS functionality was initialized in Mission Planner. After each flight, the data-flash logs of the UAV were downloaded, as well as the telemetry logs from Mission Planner.

3.4 UAV Platform Data Analysis Methods

The raw data associated with the UAV testing outlined above resulted in three major sets of data: manually recorded battery voltage, telemetry logs, and data flash logs. A combination of Python and MATLAB programs was used to analyze the data.

Prior to the start of analysis, the different sets of raw data had to be converted into a useable form. The telemetry logs from the UAV contained position data which was transmitted from the UAV to the Mission Planner. The data type of the telemetry logs was ".tlog" which was proprietary to Mission Planner. However, Mission Planner gave the capability to convert a telemetry log to a .kmz and .gpx (GPS Exchange XML Format) file formats. The .kmz file was useful for flight path visualization in Google Earth, whereas the .gpx file format could be used by many other programs. Telemetry logs from Mission Planner were saved between start up and closing of the application. Therefore, some dates had both the 30.68m and 60.96m flights in a single file. Using GPS Track Editor, these flights were separated into their own GPX files.

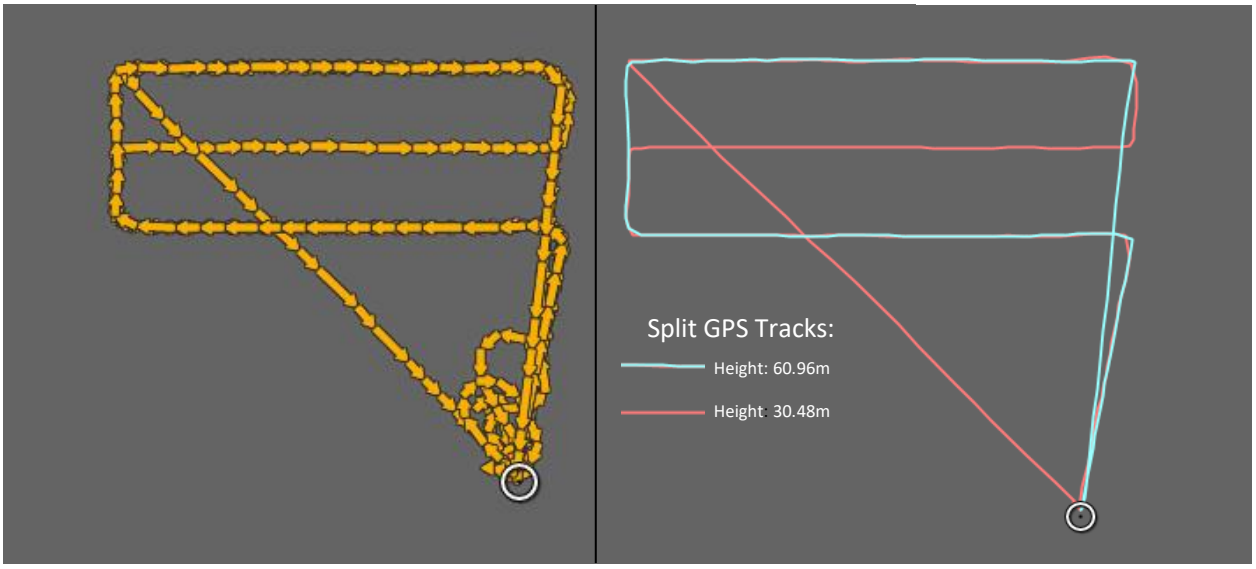

(a) (b)

Figure 5. Splitting single gpx file into separate tracks: (a) Single gpx file; (b) Two GPS tracks obtained after splitting

In Figure 5, a “manual test flight”, 30.48m mission, and 60.96m mission were shown in the same file (mission paths follow the waypoint files from). Using Geosetter, the tracks were separated and are shown in Figure 5. The red line shows the 30.48m (100ft) flight, and the blue path shows a 60.96m (200ft) flight.

The data-flash logs were stored onboard the UAV on a SD card in a .bin format. Mission Planner allowed the user to configure the information accordingly and store them in the data-flash logs when the log began recording. In this case, the dataflash log stored all position, attitude, GPS, and vibration data (among other sensor data). It was configured to start recording when the UAV was armed prior to flight (this helped keep the size of the logs down, as the other option would begin a new dataflash log for each time a battery was plugged in.) Data-flash logs were unique to each flight, because at the

end of each flight when the UAV was disarmed, the dataflash log was stored with a name of the date and time of the flight. The date and time were recorded from GPS, so it was important to note that the dataflash log would not create a unique name for indoor flights or flights without GPS. Figure 6 shows the log analyzer built in Mission Planner.

Figure 6. Mission Planner Dataflash Log Analyzer

While the log analyzer was a useful tool for tuning and troubleshooting the UAV, it did not give direct access to the data. Mission Planner also provided a tool to convert all of the information to a .mat file for MATLAB analysis. MAT files allowed the user to use MATLAB for a more thorough analysis of the data, as opposed to only a visual representation.

To analyze the lateral errors of the UAV, the desired flight path was compared to the actual horizontal (latitude and longitude) of the UAV. Lateral errors will affect image overlap percentage, which will affect the orthomosaic image accuracy. A similar approach was taken for vertical errors. Vertical error variances will affect the ground sample resolution of each image taken. Figure 7 shows a flowchart for processing the data.

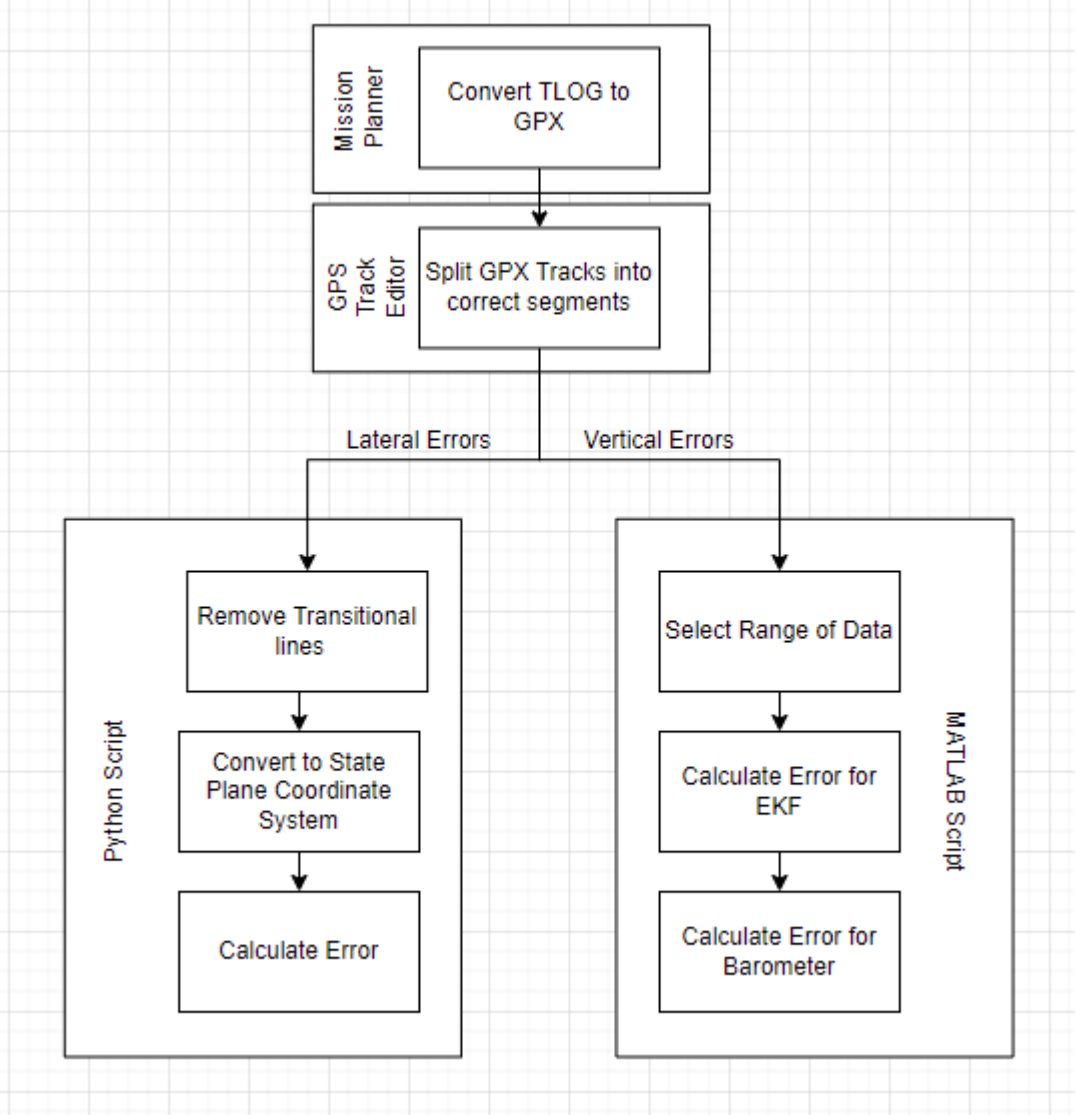

Figure 7. Data analysis method to calculate lateral and vertical errors

A program was developed using Python 3.9 for data processing. All latitude and longitude data from the GPX files were converted to state plane coordinates using the Python Stateplane library. The desired flight path was determined by the waypoint file used to command the UAV during different flights. Two different Python scripts were used to compare the different waypoint files to their associated resulting data at each altitude. Only the direct lines between waypoints in the East West direction were considered, as the transitional movements between waypoint lines are of little interest and

importance for image collection. Figure 8 identifies the transitional lines and direct flight lines.

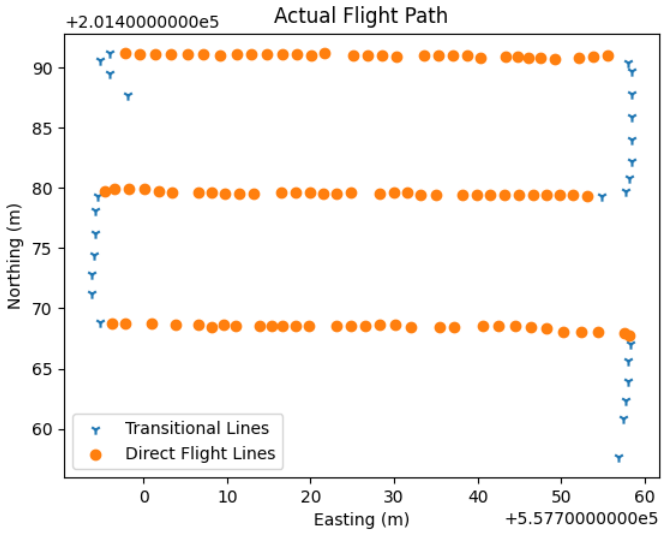

Figure 8. Actual flight path, including transitional lines and flight lines

To remove the transitional portions of the GPS data, a 1.5m threshold was used to distinguish moving in a North direction. A change greater than 1.5m would suggest the UAV was in a transitional segment. The GPS locations identified with the orange points were the GPS points which analysis was conducted on. A Python program was developed to compare the actual location in the Y direction with the desired location in Y, as defined by the waypoint selections from the flight plans. For all flights, the same waypoints were followed as outline in Figures 2 and 3. For this reason, only the latitude of the GPS points were reviewed.

To calculate error associated with the altitude, the MATLAB data files of the dataflash logs were used. The UAV recorded desired altitude, EKF altitude, as well as barometric altitude. EKF altitude was calculated through the Extended Kalman Filter, and

combined GPS, barometer, compass, accelerometer, and rate gyroscopic data to output a more certain altitude. A MATLAB program was developed to select the flight data only to analyze altitude (the altitude variations when on the ground or transferring between the home position and the first waypoint were ignored). Figures 9 and 10 show the desired altitudes, EKF, and barometric altitudes during the flight. These data points were recorded at 10Hz, which was the default setting in Mission Planner.

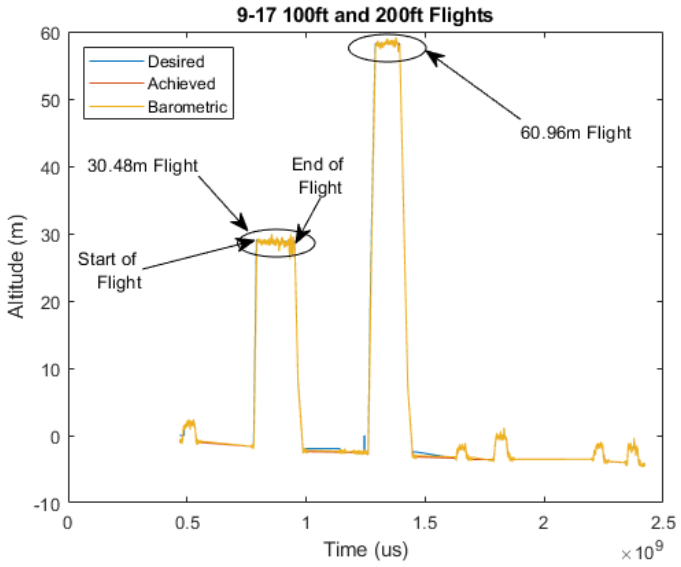

Figure 9. Altitude data from dataflash logs

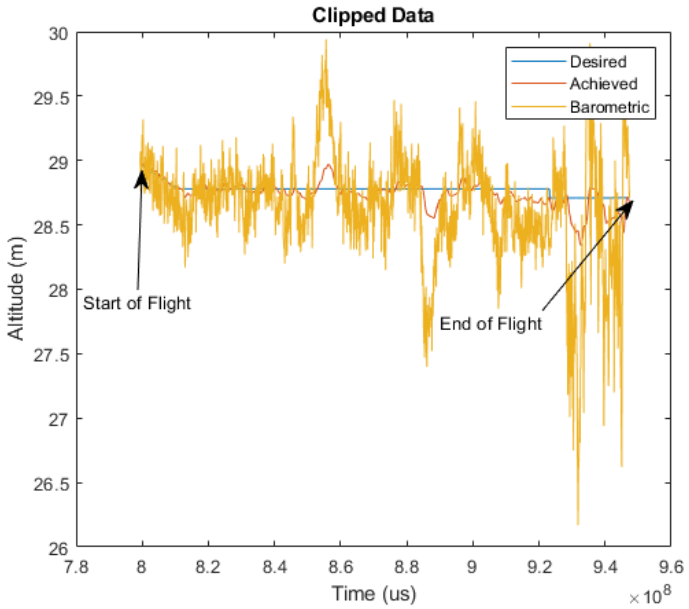

Figure 10. In-flight altitude data selected using the developed MATLAB program

Desired Altitude was the altitude commanded to the UAV by Mission Planner, Achieved Altitude was the EKF based altitude, which was actually achieved by the UAV, and Barometric was the altitude given by the internal barometer on the Cube Orange.

Errors were recorded between desired altitude and EKF altitude, as well as between desired altitude and barometric altitude. The barometer used in the Cube Orange was a MS 5611 Barometric pressure sensor, which had an advertised accuracy of 10cm. Therefore, the RTK corrected GPS position should be considerably more accurate. The desired altitude was also relative to the home position of the UAV, which changed between dates. Therefore, to maintain the desired altitude over the subject location within the field area, the desired altitude must change. Altitude data was taken over the entire flight time, including the transitional segments which were removed from the lateral error analysis.

3.5 Results and Analysis

The experiment on the UAV platform included flight time tests and flight path accuracy tests. Flight path accuracy tests relied solely on the position of the UAV vs. the desired position of the UAV. Flight time tests included the time of flight on a fully charged battery vs. the change of the battery voltage.

3.5.1 Flight path accuracy tests

The UAV platform performed extremely well during the test flights. The lateral errors are shown in Figure 11 below.

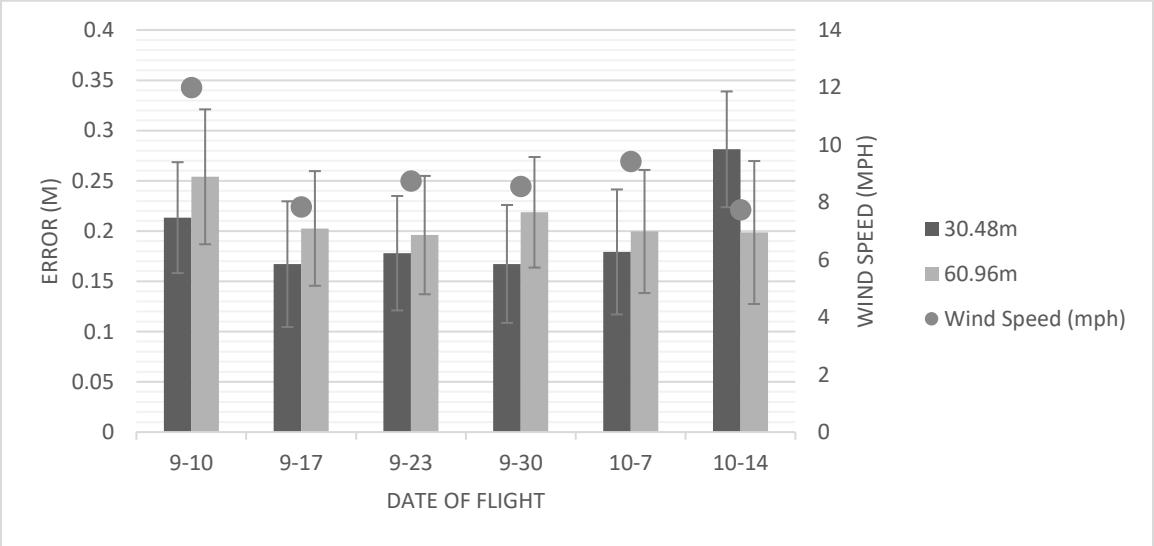

Figure 11. Lateral errors and wind speed

The average number of data points in the 30.48m flights was 102. The average number of data points in the 60.96m flights was 67. Daily average wind speed was

retrieved from the Oklahoma Mesonet Station at the Oklahoma State Ft. Cobb research station and represents the average wind speed at 10m above ground level over a 24 period. To test the effects of different flight heights across all dates, all of the collected data was pooled, and 250 points were randomly resampled to remove the environmental effects of windspeed on different dates. The data set which was resampled is shown in Figure 12.

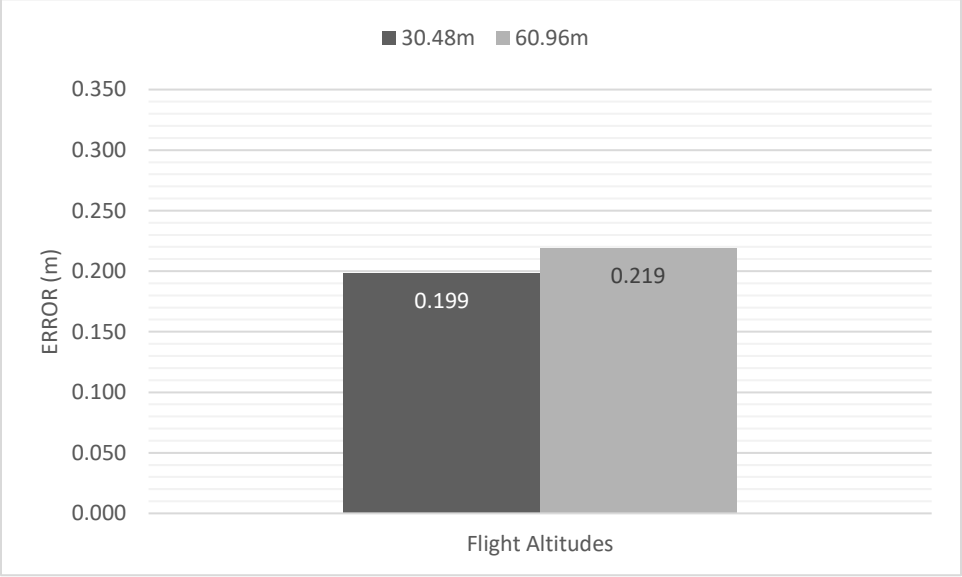

Figure 12. Lateral errors for the two flight heights after resampling

Assuming equal variances, a paired t-test was used to see if there was a statistically significant difference in accuracy between the 30.48m flights and the 60.96m flights. The results of the paired t-test showed that there was a significant difference in the average errors between dates ($\alpha = 0.05$, $t = -1.7913$, $p = .0372$). This testing showed that error increases with altitude. The vertical errors could result in a lower ground sample resolution across the set of images, which would cause less resolution in the final

orthomosaics. Altitude was recorded from the dataflash logs on the Cube Orange and contains both barometric and EKF altitude estimates. Figures 13 and 14 show the average of errors related to EKF and barometric measurements on the two flight heights.

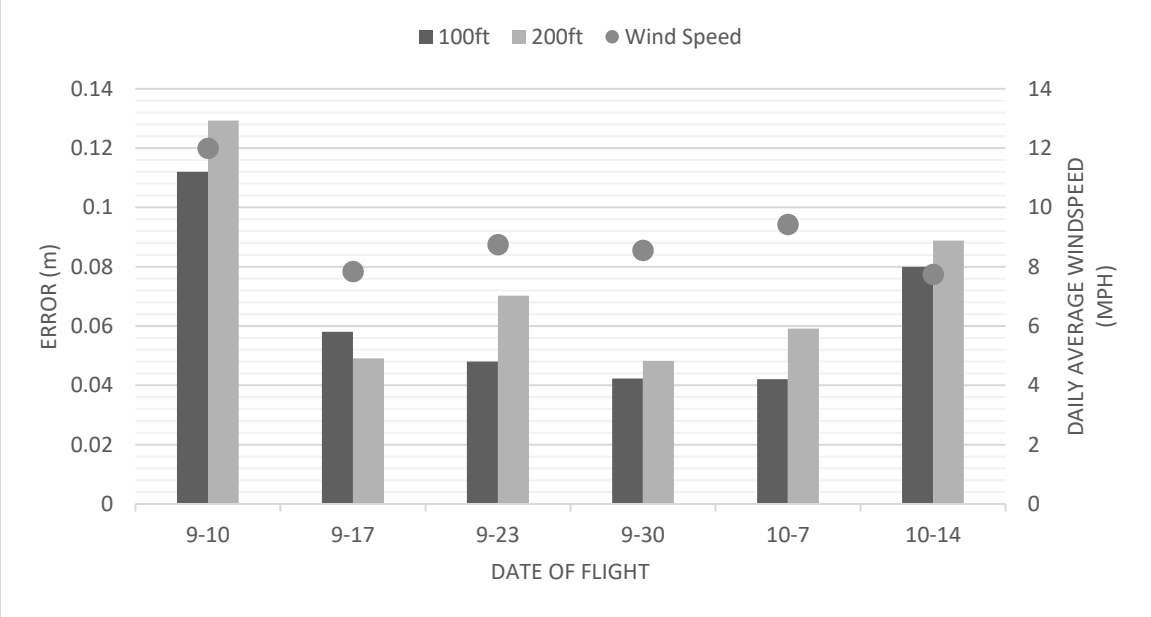

Figure 13. The average errors of the EKF altitude and wind speeds on the testing dates

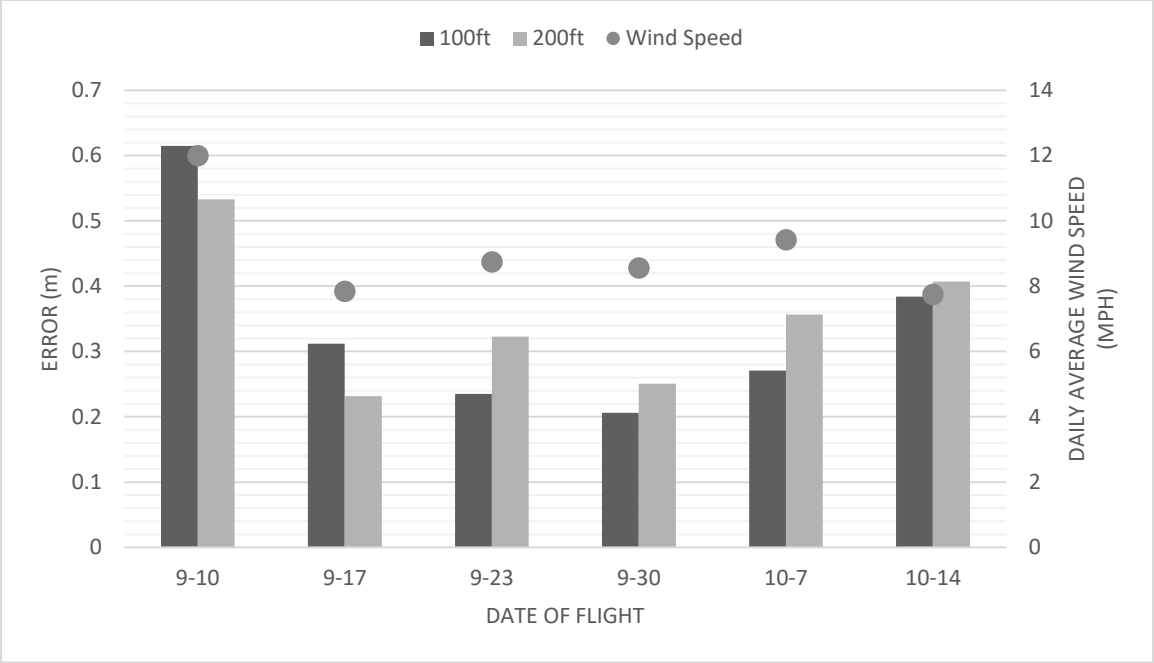

Figure 14. The average errors of the barometric altitude and wind speeds on the testing dates (date-month)

Figure 13 and 14 showed that while the data trended the same, the barometric measurements were subject to far higher errors on each flight date. Higher errors according to the barometer were due to the rated accuracy of the sensor, which was 10cm. A larger error was expected in the barometer readings. A comparison on dates between the two measurement types are shown in Figures 15 and 16 as a demonstration on relative accuracy.

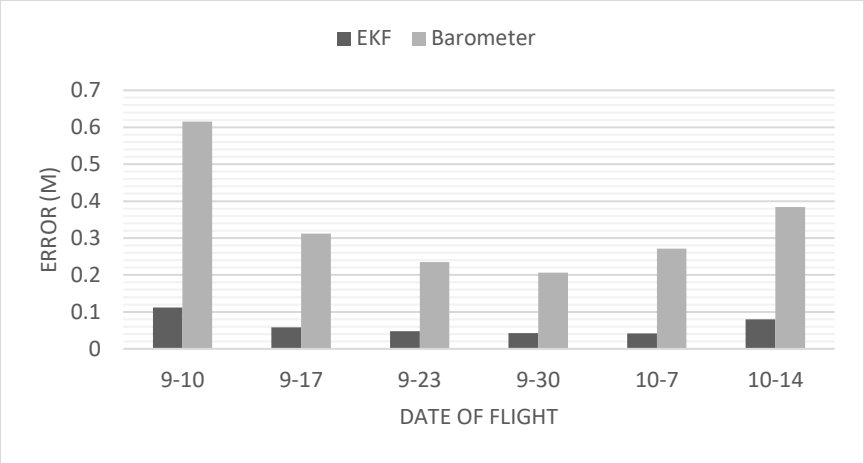

Figure 15. Comparison between the altitude errors at a flight height of 30.48m on each testing date (date-month)

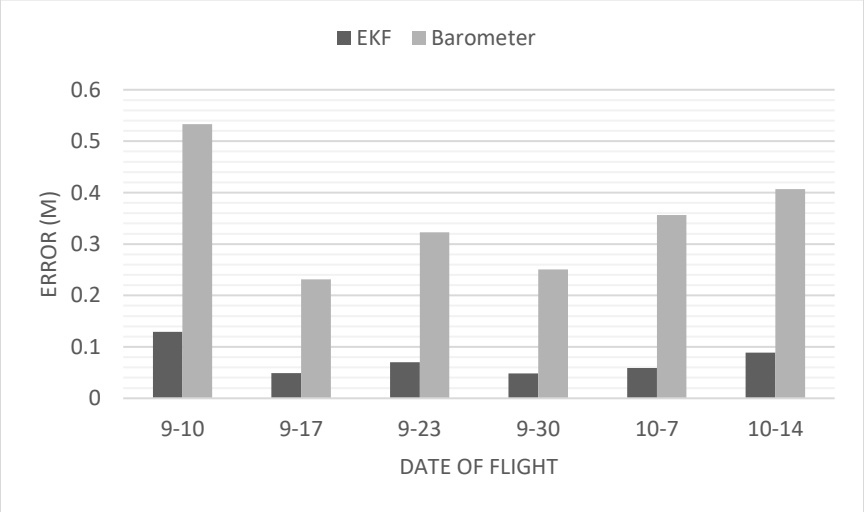

Figure 16. Comparison between the altitude errors at a flight height of 60.96 on each testing date (date-month)

The barometer errors were far larger than the EKF errors across all the dates and at both altitudes.

A paired t-test was used to evaluate the difference in average errors between altitude errors at the two flight heights. Similar to the lateral error calculations, all altitude data was combined and randomly re-sampled. Two thousand data points were resampled

from the altitude data. The results of the re-sampled data are shown in Figure 17 and Figure 18.

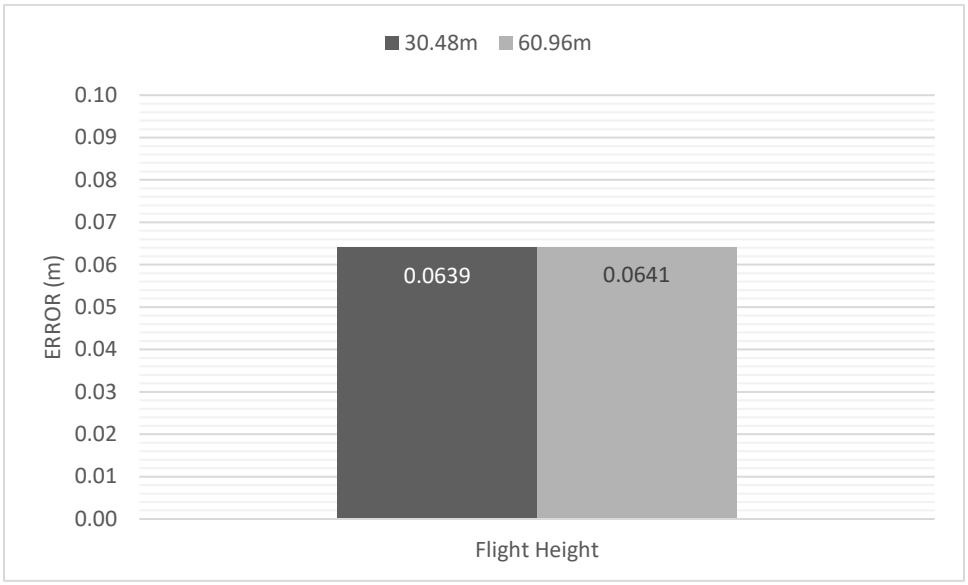

Figure 17. EKF altitude errors at the two flight heights after resampling

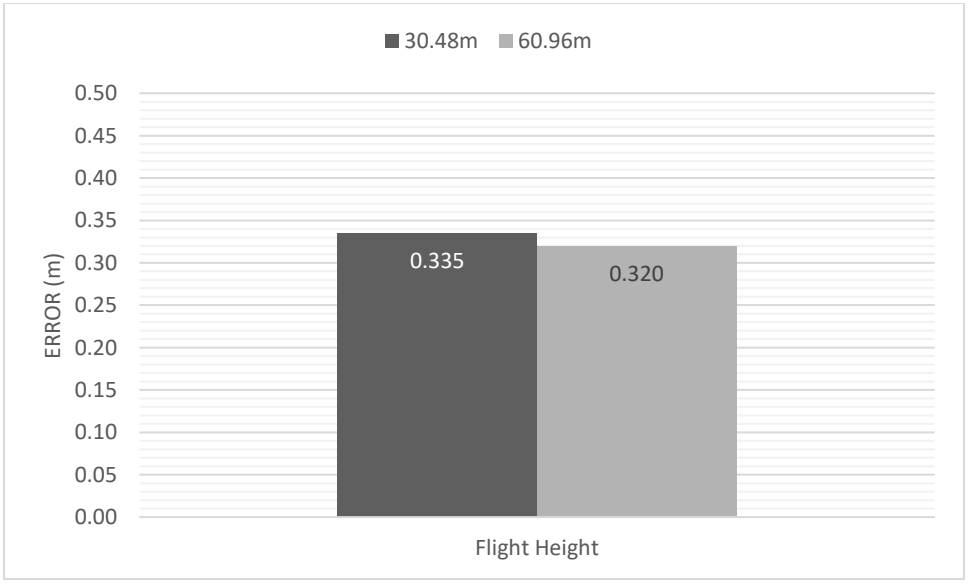

Figure 18. Barometric altitude errors at the two flight heights after resampling

Finally, a paired t-test was performed between flight heights on barometric altitude data and EKF altitude data. The EKF test showed that there was no difference in the mean EKF altitude error ($\alpha = 0.05$, $t = -0.102$, $p = .459$). The barometric test showed that there was no difference in mean barometric altitude error ($\alpha = 0.05$, $t = 1.352$, $p = .08$). High probability values shows that while there is a possibility of a different average error in both tests, there is not sufficient evidence to reject the null hypothesis.

3.5.2 Flight time tests

Battery voltage was recorded at the start and the end of each flight. To compare flight times between dates, a flight time index was used with a unit of voltage per minute. This index was calculated as the difference between the voltages at the starting and the ending time divided by the time the UAV was in flight. Figure 19 shows the flight time index on each testing date.

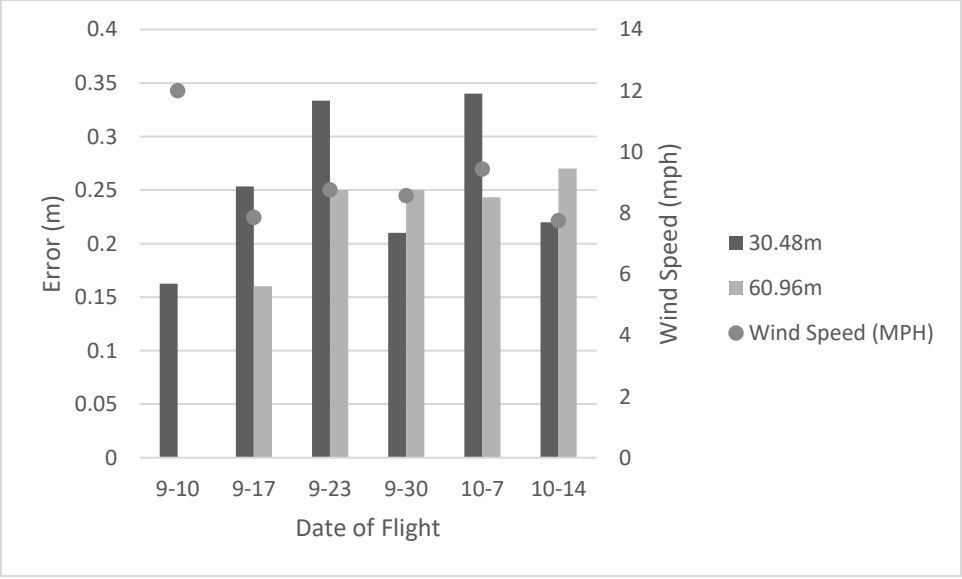

Figure 19. The flight-time index in Volts/Minute and Windspeed

The cumulative average voltage/minute across all dates and altitudes was 0.244 volts/min. This correlated to roughly an 8-minute flight time if the UAV was stopped with 25% battery life remaining. This was a measurement for a single battery, whereas the UAV had the capability to carry two 9000mAh batteries. This measurement was also an average across multiple dates, and included lift-off, landing, and transitional time periods.

3.6 UAV Testing Conclusions

The UAV performed well during testing, with the greatest lateral error being found at higher altitudes. Flight height had no effect on the vertical error according to the barometer data of the UAV during flights. The test on altitude error according to EKF data had a large p value ($p = .459$), therefore the conclusion of a higher error at higher altitudes is not significant. Further testing should include an analysis of GPS accuracy prior to the data being pooled together. Table 1 shows the summary of the results from the statistical tests.

Table 1. Summary of the UAV testing results

Test	Type of Test	Results	α	Test Value	*p*
Flight heights effects on lateral error	Paired t-test	Error increases with altitude	0.05	t = -1.791	0.037
Flight heights effects on vertical error (EKF)	Paired t-test	No result	0.05	t = -0.102	0.459
Flight heights effects on vertical error (barometer)	Paired t-test	Error does not increase with altitude	0.05	t = 1.352	0.080

The battery tests resulted in an average battery use of .25v/minute of flight. This was measured with a payload of three complete cameras and uses a 9000mAh battery. The UAV had the capacity and room to mount an additional 9000mAh battery, which should increase flight time. However, further testing needs to be conducted to analyze the difference in flight time with multiple loads. Table 2 shows the specifications of the UAV platform.

Table 2. UAV Cost List

Component	**QTY**	**Unit Cost (US$)**	**Item Cost (US$)**
Frame	1	170	170
Motors	6	54	324
ESCs	6	25	150
Props	6	5	30
Landing Gear	1	40	40
Cube	1	300	300
GPS	1	150	150
Flight Controller	1	170	170
Radios	1	90	90
Batteries	1	70	70
PDB	1	19	19
Misc.	1	150	150
Total Cost			*1663*

Table 3. UAV Specifications

UAV Specifications	
All Up Weight	2.83kg
Height	44cm
Width	1m
Flight Time	8 Minutes (at max payload)

Payload	1.5kg

CHAPTER IV

DEVELOPMENT OF A TWO AXIS GIMBAL FOR THE UAV PLATFORM

4.1 Design Goals

As noted in the review of literature, most data acquisition techniques for UAVs rely on a gimbal of some kind to stabilize the cameras or sensors to stay perfectly horizontal during movement of the UAV. To stay within the scope of this project, a 2-axis gimbal was designed and constructed. While 3-axis gimbal with brushless motors have been more commonly used for UAVs to collect video data, they have many drawbacks. Firstly, they are heavy comparatively to a 2-axis servo gimbal. Secondly, they are usually limited to carry a single camera. Thirdly, in downward facing mapping missions (such as those over research plots and other fields) the sensors on the gimbal are heavily affected by the yaw motion of the UAV (as many post processing programs are able to transform images), therefore negate the use of the 3rd axis of a 3-axis gimbal. Brushless motors generally have a higher accuracy, but the effects between a brushless device and servo device are mostly notable when a video is taken. In the case of a mapping UAV, videos will likely be dismissed in favor of single-shot images. Lastly, a brushless gimbal requires its own control board, whereas a servo gimbal can

be directly controlled by the Cube Orange via two of the six on-board auxiliary PWM outputs. Based on all these considerations, a 2-axis gimbal should offer significant advantages over a 3-axis gimbal, in terms of simplicity, cost, and flight time.

4.2 Design and Construction

While there were several 2-axis gimbal options available, it was determined that fabricating one would be a simpler solution. Figure 20 shows the initial design of a 2-axis gimbal for multiple cameras.

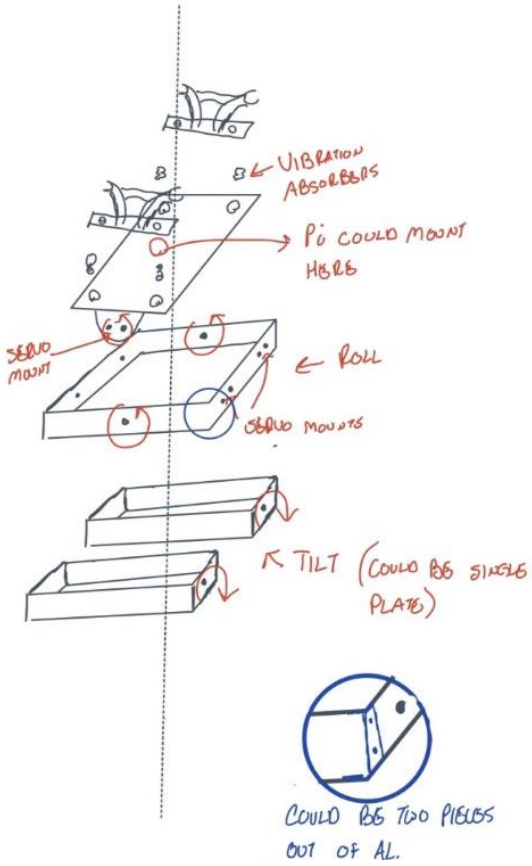

Figure 20. Initial design of 2-axis servo driven gimbal

The initial design used three servos in total, where each camera mount had a dedicated tilt plate and servo. This design was modified so that a single tilt plate would be controlled by a single servo. This could save weight and complexity of the design. The roll direction required more force to move, due to the weight of the pitch section, tilt plate, and servo involved. The pitch direction would only control the tilt plate and camera mounts. Despite this, the same two servos were used in the design to minimize complexity.

To account for weight, as well as accessibility for future upgrades to stay within the guidelines of an open-source project, the gimbal was designed with readily accessible aluminum from a hardware store, common fasteners, and 3-D printed components. Fabrication techniques included simple 90-degree bends, drilling holes of common sizes, and paint. The gimbal was design to hang directly under the body of the UAV by clamping on the horizontal carbon fiber tubes provided with Tarot kit (UAV Systems International, Nevada, USA). Table 2 shows the materials list and prices.

Table 4. Materials List for the Designed Gimbal

Name	**Quantity**	**Unit Price**
1/16”x1” Aluminum Flat (6063-T5)	6ft	$11.48
Goolsky 20kg Digital Servos	2	$17.99
Tarot Camera Gimbal Suspension Hooks	2	$6.99
Assorted M2.5 Fastener Kit	1	$11.99
Vibration Dampener Kit (pack of 6)	2	$8.85

The 3D printed components were created out of ABS plastic, provided by the Endeavor Laboratory at Oklahoma State University, in Stillwater, Oklahoma. The camera mounting solution was provided via an undergraduate research project, with parameters provided to the undergraduate student being a minimum capacity of three cameras, fast camera swapping solutions, and reconfigurability. Figure 21 shows the completed gimbal installed on the UAV.

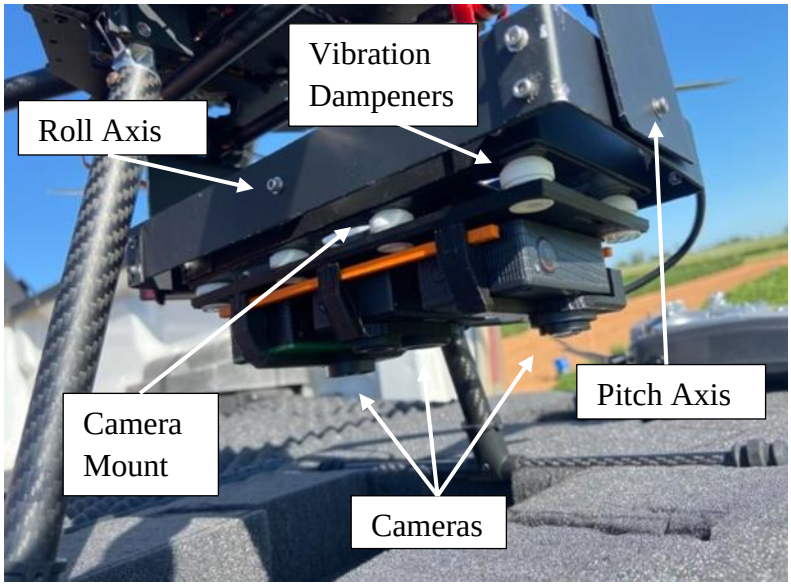

Figure 21. Completed gimbal

The vibration dampers helped to minimize the effect of vibrations in flight. The two orange components slide in to lock all three cameras in place. Each of the mounting solutions for the cameras were independently designed and printed, but the fastener solution was common to all, which allowed the end user to simply 3D print a mount for any style camera to be carried.

4.3 Testing Methods and Criteria for evaluating the Gimbal Platform

The gimbal's function was to ensure that as the UAV performed pitch and roll movements, the cameras remained facing in a downward position horizontally. To test

the gimbal performance, an Arduino Nano Microcontroller (Arduino, Italy) was used to read two MPU6050 3-axis accelerometers coincidentally and write the data to an SD card. A momentary button was used to run a calibration procedure on the accelerometer and a 5V digital output on the UAV was used to trigger the Arduino data logger. Figure 22 shows a block diagram of the data acquisition system.

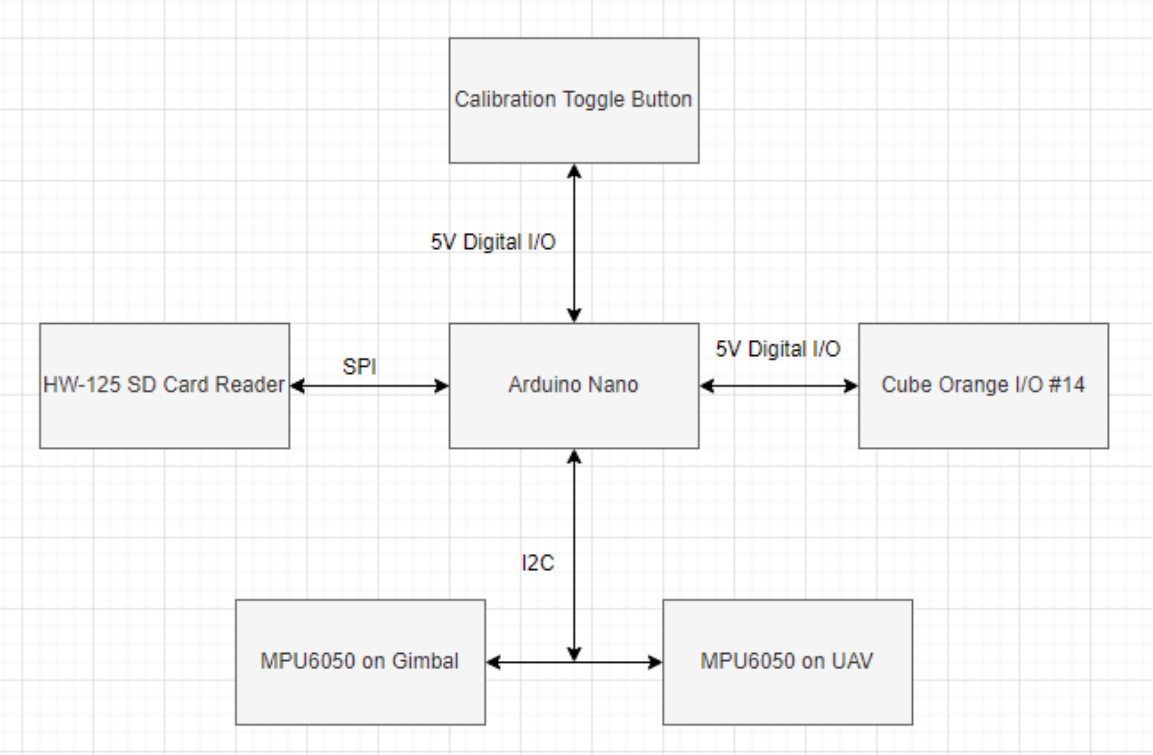

Figure 22. A block diagram for a test setup to evaluate the performance of the gimbal platform

The data logger circuit was mounted to the UAV and powered via a regulated 12V power source provided by the UAV's power distribution unit. One accelerometer was mounted to the gimbal, and one accelerometer was mounted to the top mounting plate of the UAV. As the UAV performs pitch and roll maneuvers, the gimbal should remain relatively close to level horizontally. Only two of the three axes of the accelerometers were recorded to save computational power and speed up the process.

One of the Cube Orange's outputs was set to be a relay signal, and the relay was mapped to a toggle switch on the RC controller. An additional momentary button on the Arduino circuit was used to trigger calibration procedures for the accelerometers. Figure 23 shows the circuit installed on the UAV.

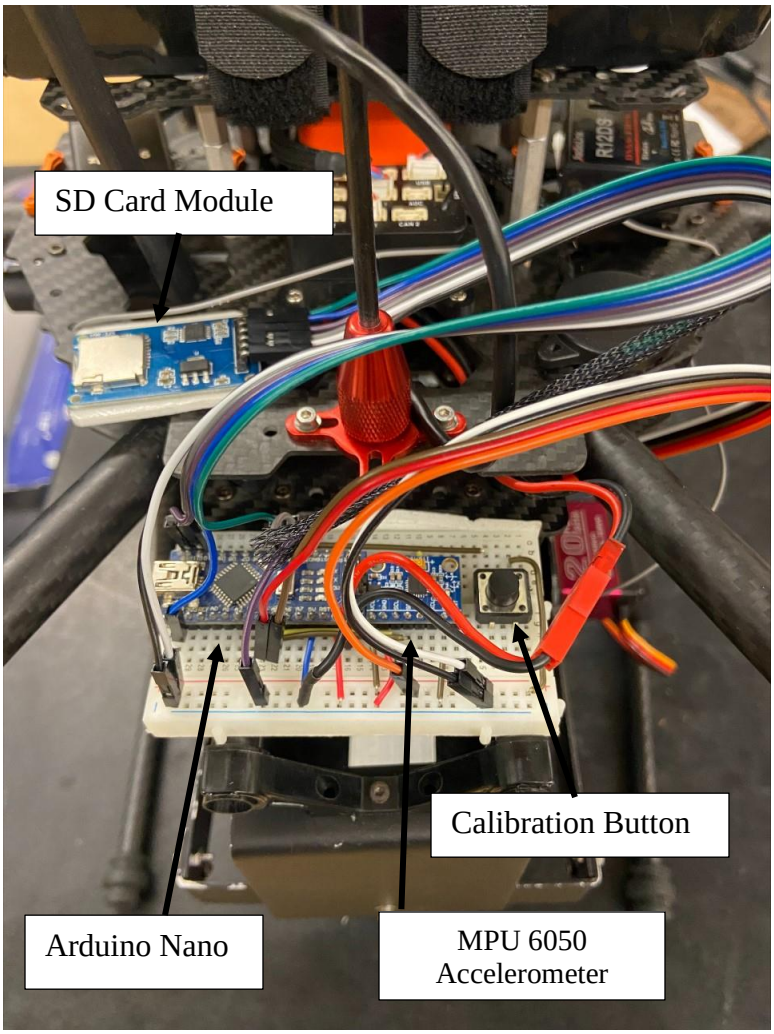

Figure 23. Data logger circuit installed on UAV

A calibration was necessary between all tests to zero the angles of the accelerometers. In several bench tests, the data collection rate was 20Hz for pitch and roll of both accelerometers.

The following steps were followed during the gimbal performance tests after the UAV was powered.

1) Connect the Arduino circuit;
2) Press the momentary button in the Arduino circuit to calibrate accelerometers;
3) Turn on the toggle switch to start data logging;
4) Pick up the UAV and move in roll and pitch directions up to +/- 25 degrees;
5) Turn off the toggle switch to stop data logging and save the collected accelerometer data to a CSV file;
6) Disconnect the power to the Arduino circuit;
7) Remove the SD Card and copy the data to a computer; and
8) Re-insert the SD card to the datalogger.

In each test, the time since the Arduino microcontroller was booted up in milliseconds, the pitch of UAV, the roll of UAV, the pitch of gimbal, and the roll of gimbal were recorded.

To test the gimbal under different conditions, three different weights and two different mounting styles were tested. Figure 24 below shows the different configurations which can be used with this design.

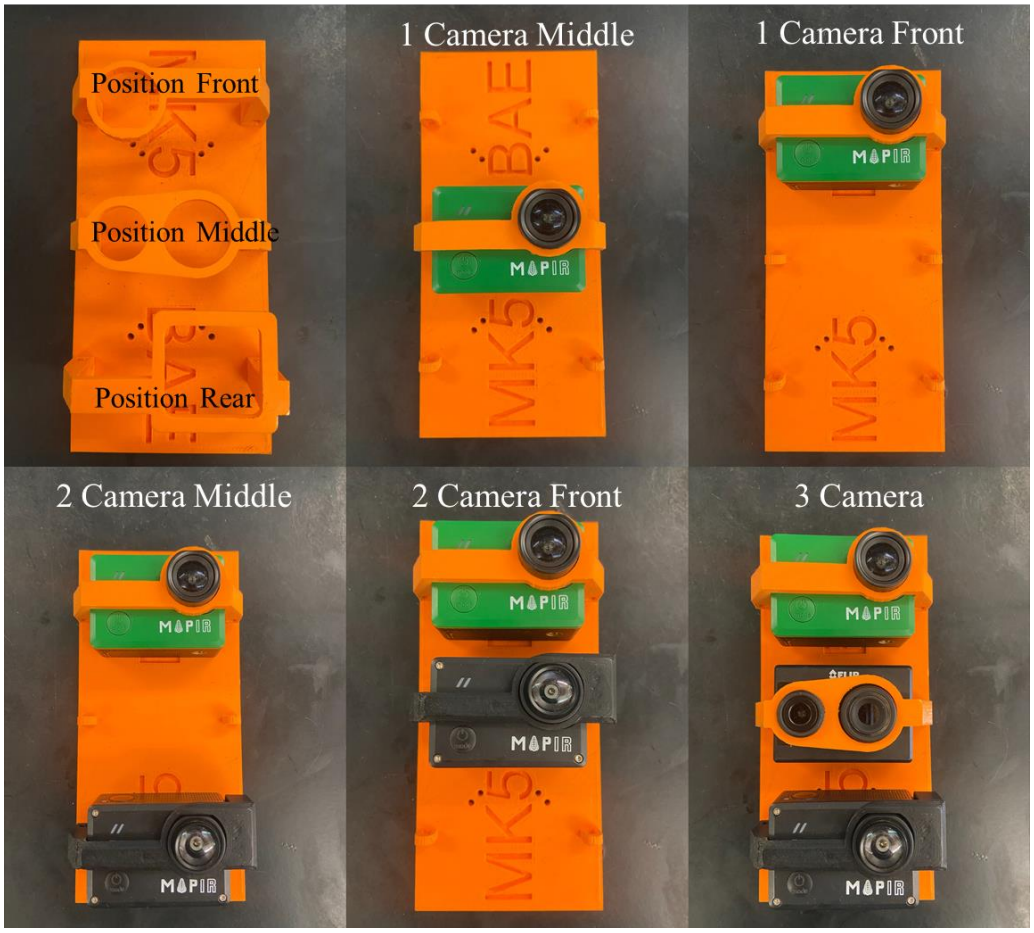

Figure 24. Different Possible Camera Configurations (The orange plate was the camera mounting plate.)

The tests included five treatments (camera mount configurations) and three repetitions of each test for a total of 15 tests. The main goal of these tests was to evaluate the gimbal responses for each of the configurations. Each camera was less than 100 grams in weight. The front mounted tests were helpful in determining if centering the load on the gimbal had any effect on stability and accuracy.

Test criteria included the pitch and roll of both the UAV and the gimbal, respectively, in degrees. The results of these tests should be an average error in degrees in

each direction. The gimbal error in each direction equal to the angle measurement as given by the accelerometer using a complimentary filter in the built in Arduino Library.

4.4 Gimbal Platform Data Analysis Methods

To analyze the data from the gimbal tests, a MATLAB program was developed to read the data stored in each CSV file, performed calculations for the mean and standard deviation in both pitch and roll directions, count the number of data points recorded. It is important to note that the data collected from the data logger contained both positive and negative values which were related to the directions along that axis. The mean values reported. Figure 25show an example of the raw data and the calculated error between the two accelerometers.

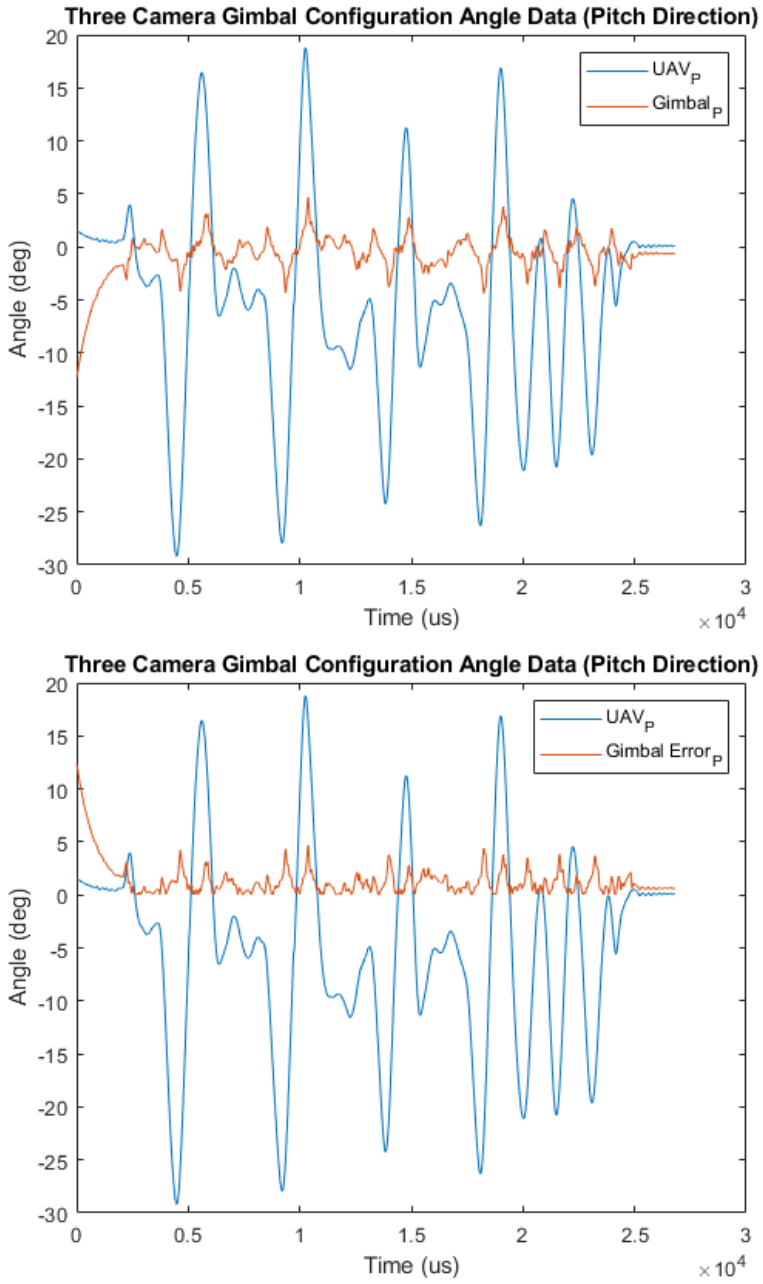

Figure 25. Example of the calculated absolute error between the data from the accelerometer on the gimbal and the accelerometer on the UAV

The MATLAB program output the summary statistics for each test and repetition, which was then copied into Excel for storage and data analysis. Weighted average and standard deviation were calculated in Excel for each test with Equation 4, 5, and 6.

$$W = \frac{\sum_{i=1}^{n} w_i X_i}{\sum_{i=1}^{n} w_i} \quad (4)$$

$$w_i = \frac{N_i}{\sum_{i}^{n} N} \quad (5)$$

$$Average\ Standard\ Deviation = \sqrt{\frac{\sum_{i}^{n} (N_i - 1) {s_i}^2}{\sum_{i=1}^{n} N - n}} \quad (6)$$

where i was the repetition number, X_i was the mean of all data collected for that trial, w_i was the weight of the sample set, N_i was the number of samples in a single repetition, N was the sum of all samples in a single test, s_i was standard deviation of a single repetition; n was the number of repetitions, and W was the weighted average.

The average standard deviation formula used was for un-even sample size, which was the case in all of the tests.

4.5 Gimbal Testing Results

The gimbal testing results included the effects of different weights and mounting configurations on gimbal accuracy in the roll and pitch directions. In the 3 camera configuration (which is the desired configuration of the gimbal in most conditions), response time was analyzed. Figure 26 below shows an example of response time in the roll direction.

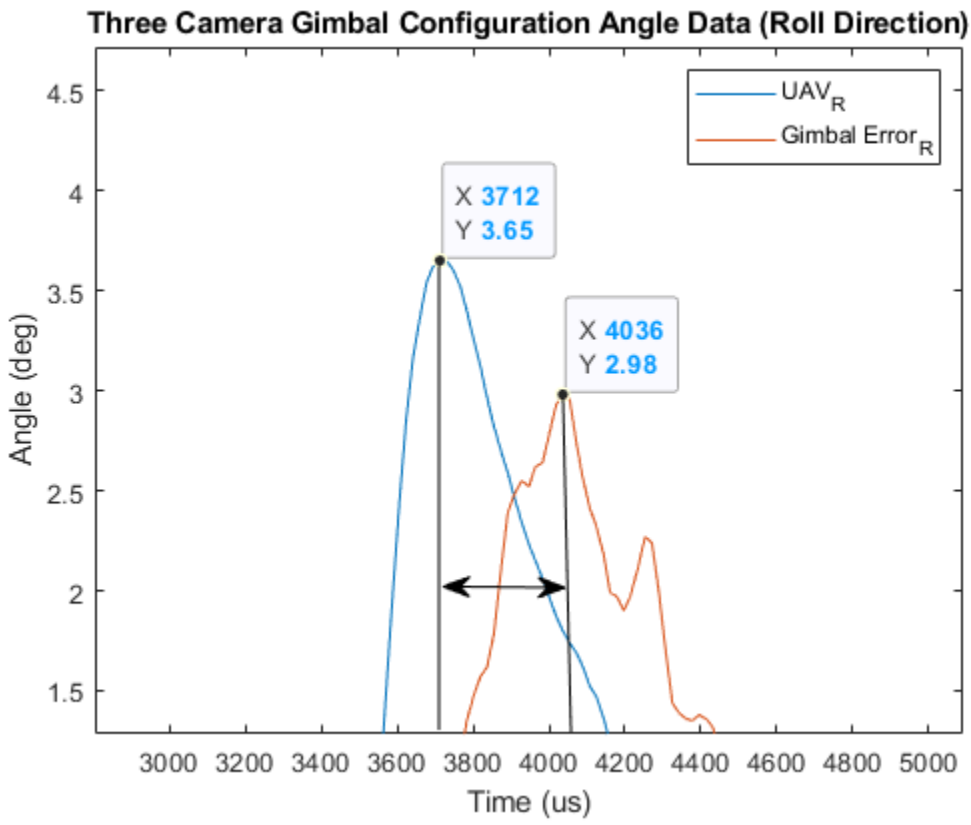

Figure 26. Response time of gimbal in roll direction

The average response time in the roll direction was 199 microseconds, and the average response time in the pitch direction was 152.69 microseconds.

Figures 27 and 28 show the average errors associated with different camera mounting solutions in both the pitch and roll directions. The average angular errors for each test were the weighted averages of the three repetitions in that the corresponding test.

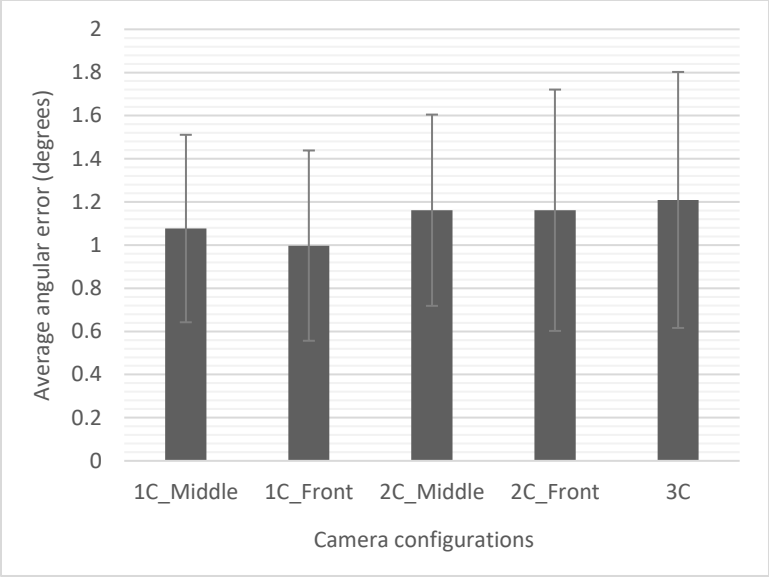

Figure 27. Results of the average errors in pitch direction for all five camera configurations

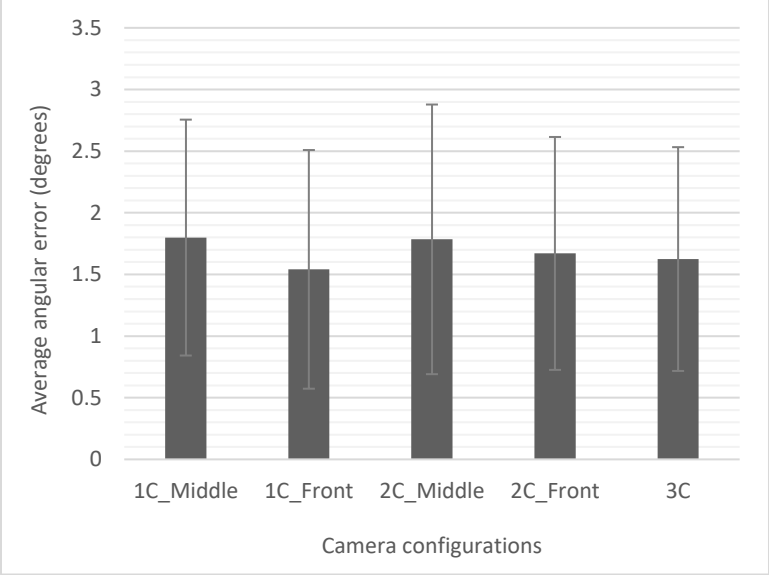

Figure 28. Results of the average errors in roll direction for all five camera configurations

Analysis of Variance was performed on both the roll and pitch directions. In the pitch direction, the results were a difference in averages existed ($\alpha = 0.05$, $F = 41.7804$, $p < .001$). The roll direction also showed that a difference in averages existed between treatments ($\alpha = 0.05$, $F = 8.982$, $p < .001$).

After finding out that the differences in the means existed among different mounting configurations, further analysis of variance was carried out on the “balanced” gimbal treatments. The balanced gimbal treatments are the “1C Middle” and “2C Middle” configurations seen in Figure 24. Figure 29 shows the average error in both directions.

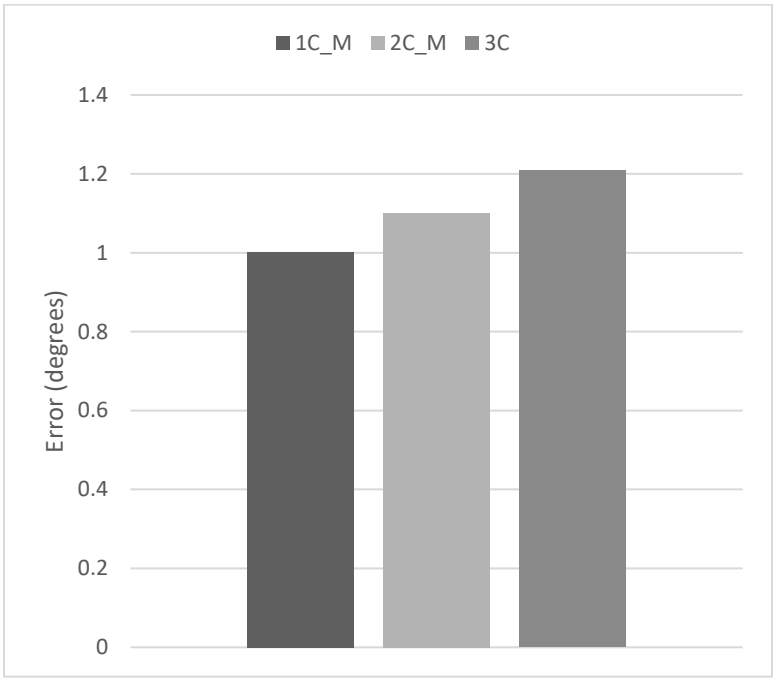

Figure 29. The average errors in the balanced configurations in the pitch direction

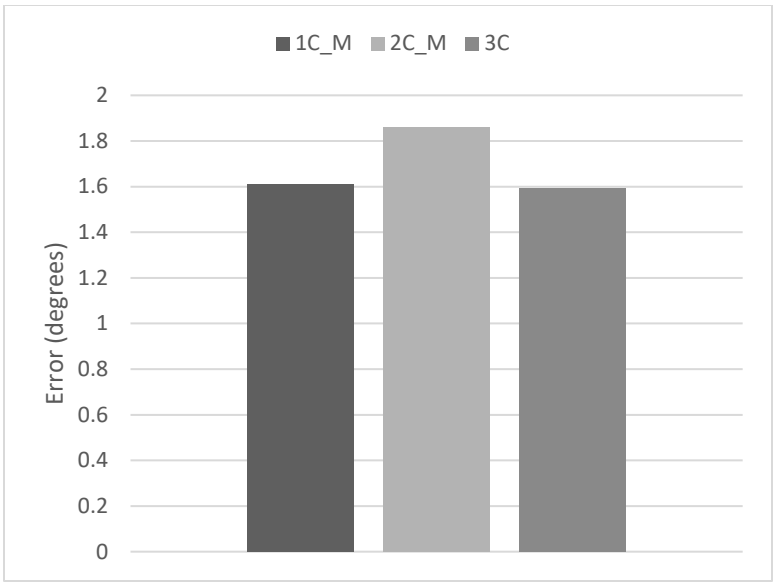

Figure 30. The average errors in the balanced configurations in the roll direction

The results of ANOVA in the pitch direction show that there was a difference in the mean errors in the pitch direction, even when the gimbal is balanced ($\alpha = 0.05$, $F = 21.363$, $p < .001$). Similar errors were found in the roll direction ($\alpha = 0.05$, $F = 10.18$, $p < .001$.)

The final analysis performed on the gimbal data was to determine if there was an increase in errors based on the balance of the gimbal. For these tests, the middle and front ("M" and "F") variants were used as treatments for a paired t-test on single camera and double camera configurations, in both the pitch and roll directions. Front vs middle mounting is in essence whether or not the gimbal is balanced around the pitch axis center. Figures 31 and 32 show the average errors between each mounting type (front or middle mounting) in the pitch direction.

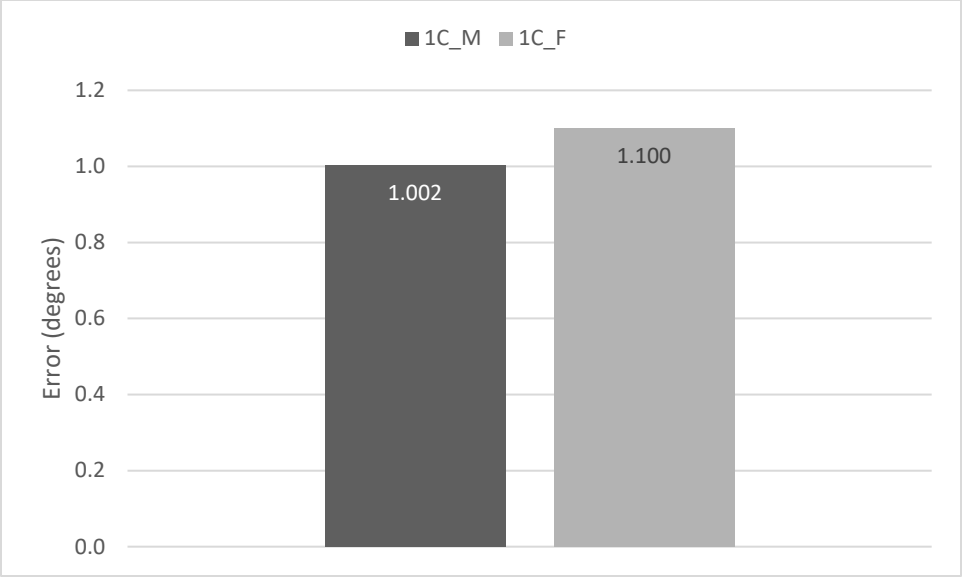

Figure 31. The average single camera errors in the pitch direction

For single camera configurations in the pitch direction, there was an increase in the error by mounting a single camera at the front of the gimbal versus mounting the camera in the center ($\alpha = 0.05$, $t = -3.533$, $p < .001$).

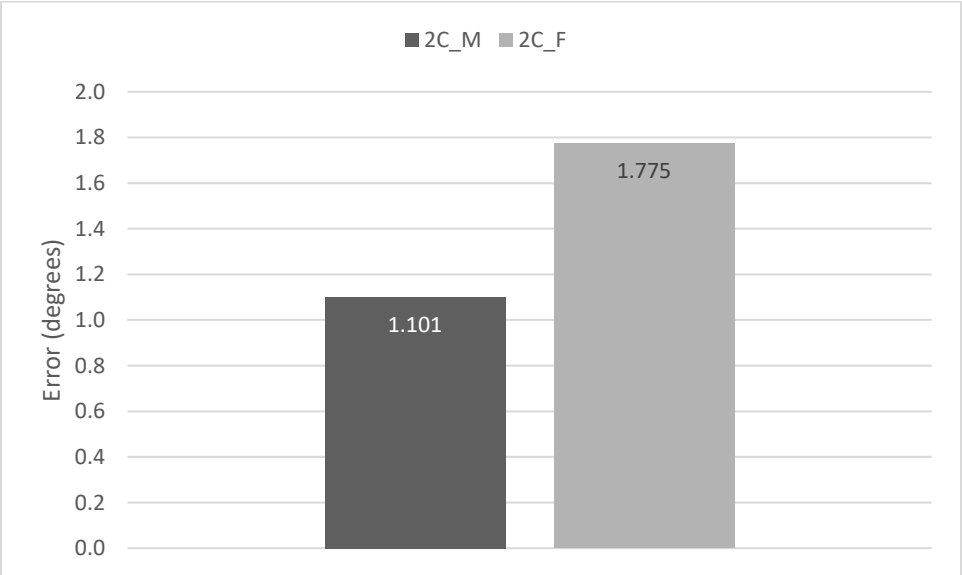

Figure 32. The average errors for two-camera configuration in the pitch direction

Figures 32 and 33 show the average errors both camera configurations in the roll direction. There was an increase in error by mounting the two cameras offset on the gimbal versus mounting them at the opposite ends (α= 0.05, t = -6.729, p < .001).

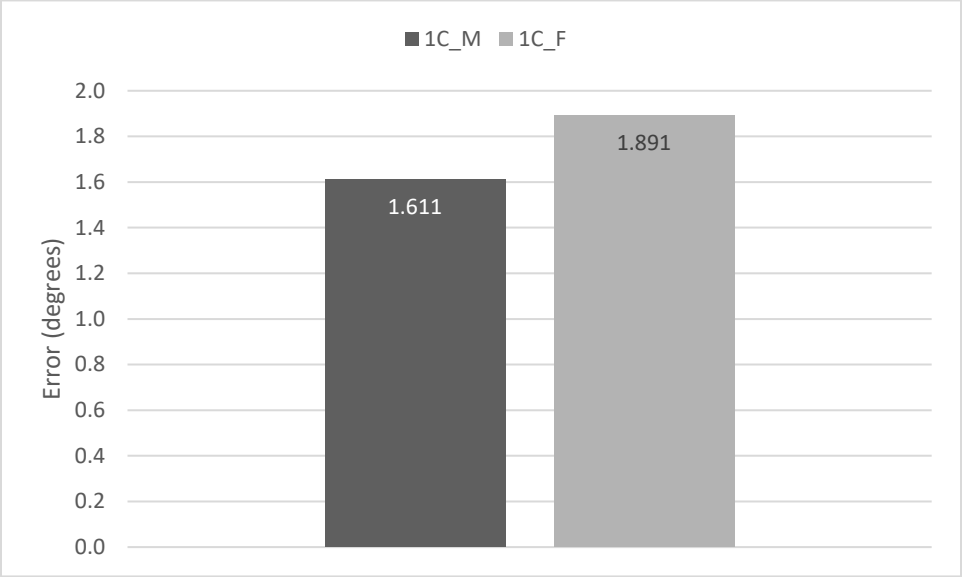

Figure 33. The average errors for single camera configuration in the roll direction

For single camera configurations in the roll direction, there was an increase in error by mounting the camera towards the front versus mounting the camera in the center (α = 0.05, t = -4.423, p < .001).

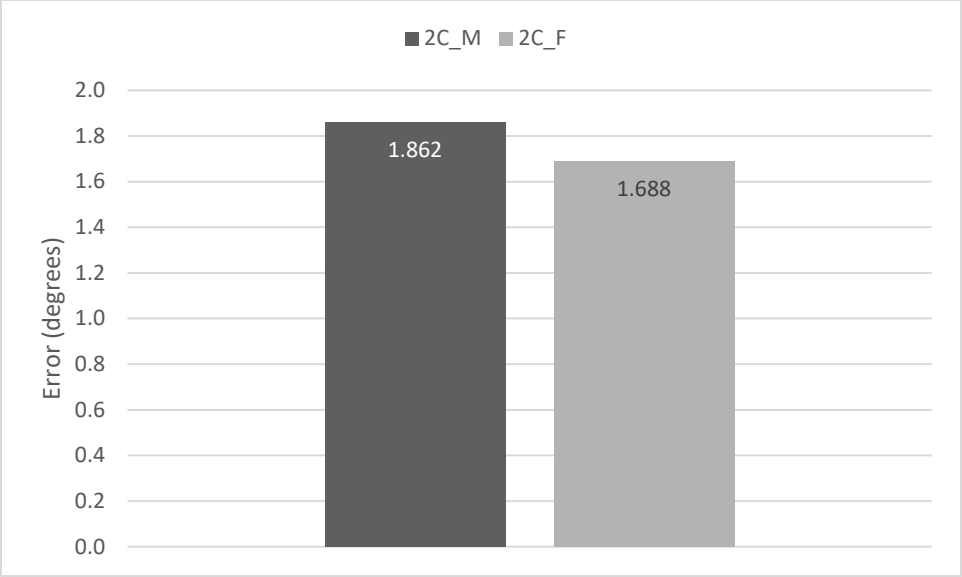

Figure 34. The average errors for the two-camera configuration in the roll direction

For double camera configurations in the roll direction, there was a decrease in the error by mounting the cameras towards the front versus that when mounting the cameras on opposite ends ($\alpha = 0.05$, $t = 2.487$, $p = 0.006$). This could be due to different center of gravity in the cameras themselves. For the case of a mapping UAV, pitch direction accuracy was of greater importance than roll direction. The pitch direction would undergo the largest changes during flight, because the UAV should be headed "forward" relative to the frame when undergoing mapping missions. In this situation, the gimbal would experience greater changes in the pitch direction than the roll direction.

4.6 Discussion on the Results

Gimbal analysis showed that any configuration led to a different accuracy. The best accuracy was found with a single, centered camera with an average of ~1 degree in the pitch direction and ~1.6 degrees in the roll direction. Mounting locations had an effect

on the accuracy of the gimbal as well, with the pitch direction having a larger error when the cameras were mounted off center towards the front. The roll direction had a larger error when mounting a single camera towards the front. The roll direction had a smaller error when mounting two cameras towards the front of the UAV, which could be due to the effects of the cameras individual center of gravity. Table 3 shows a summary of the results from the gimbal performance test, and Table 4 shows the specifications of the completed gimbal.

Table 5. Summary of the Gimbal Testing Results

Test	Type of Test	Results	α	Test Value	*p*
Pitch Direction (all configurations)	ANOVA	Difference in Averages Exist	0.05	F = 41.7804	<.001
Roll Direction (all configurations	ANOVA	Difference in Averages Exist	0.05	F = 8.982	<.001
Pitch Direction (configurations 1C_M, 2C_M, 3C)	ANOVA	Differences in Averages Exist	0.05	F = 21.363	<.001
Roll Direction (configurations 1C_M, 2C_M, 3C)	ANOVA	Difference in Averages Exist	0.05	F = 10.18	<.001
Pitch Direction 1C_M - 1C_F	Paired t-test	Difference in Averages Exist	0.05	t = -3.533	<.001
Roll Direction 1C_M - 1C_F	Paired t-test	Difference in Averages Exist	0.05	t = -4.423	<.001
Pitch Direction 2C_M - 2C_F	Paired t-test	Difference in Averages Exist	0.05	t = -6.729	<.001
Roll Direction 2C_M - 2C_F	Paired t-test	Difference in Averages Exist	0.05	t = 2.487	0.006

The effects of mounting the cameras forward on the gimbal negatively impacted accuracy. There was a change in accuracy based on camera mounting locations across all balanced testing. The average error for 3 cameras mounted to the gimbal was 1.2 degrees in the pitch direction, and 1.7 degrees in the roll direction.

Table 6. Gimbal specifications

Weight	454g
Size	12.7 x 26.5 cm
Max Pitch Angle	40°
Max Roll Angle	40°
Payload Capacity	700g

CHAPTER V

CASE STUDY: AN OPEN-SOURCE PIPELINE FOR PROCESSING COTTON CROP IMAGES COLLECTED WITH THE DEVELOPED UAV PLATFORM

5.1 Introduction

The purpose of this case study was to demonstrate a free, primarily open-source methodology for processing images collected using the developed UAV platform. In this study, the UAV was used to collect data over a cotton maturity timing trial. The trial was conducted at the Oklahoma State University Caddo Research Station in Ft. Cobb, Oklahoma. The images collected and used were captured simultaneously to the data used in the previous chapters. Data collected could be used in the future to perform a full analysis on the cotton crop; however, this study will focus primarily on the techniques needed to put the data into a useable format for analysis.

The goals of this study are listed below:

1) Geolocated images with the telemetry logs of the UAV in post processing
2) Create orthomosaics from the geolocated images
3) Align the orthomosaics across different dates
4) Extract individual plots from orthomosaic

Several open-sourced or freeware packages were used in the development of the pipeline. The software names and uses are listed in Table 7. Figure 35 shows a flowchart of the image processing pipeline.

Table 7. Open-source software packages used

Name	Use
Mission Planner	Converting TLOG files into GPX files
GPS Track Editor	Splitting GPX files into correct GPX tracks
GeoSetter	Geo-referencing photos
WebODM	Creating Orthomosaics
QGIS	Aligning Orthomosaics and Extracting Individual Plots
Python	Image Analysis and Data Extraction

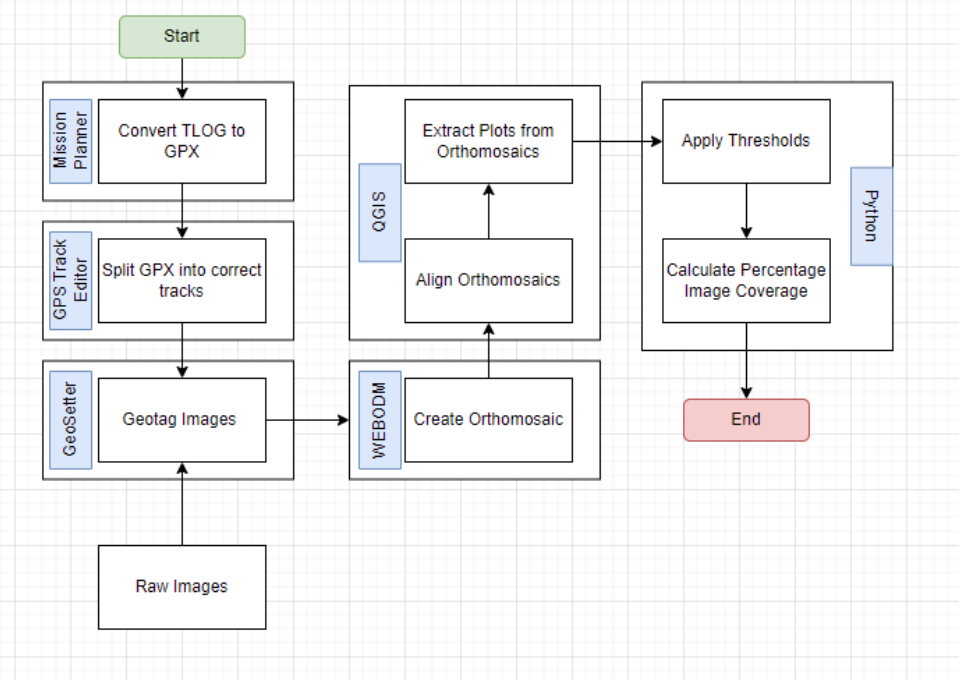

Figure 35. Image processing pipeline

5.2 Data Collection Process

The data was collected during the same flight times and using the same flight paths as described in Chapter 3. Six flights were taken at a height of 30.48m (100ft) and six other flights were taken at the height of 60.96m (200ft). Prior to each flight, the UAV was placed on a landing mat, MAVLINK data connection to the ground control station was verified, and all cameras were turned on. Camera time was verified to be close to the actual time of flight. Cameras were then activated to take images at regular intervals using a timer. The major configurations for the cameras used are shown in Table 5.

Table 8. Major Configurations for the Cameras Used in the Study

Camera	Resolution	Interval
Mapir Survey2 Red+NIR (MAPIR, California, USA)	16MP (4608x3456)	3s
Mapir Survey3W RGB (MAPIR, California, USA)	12MP (4000x3000)	2.75s
FLIR Duo R (FLIR Systems Inc., California, USA)	160x120	3s

As a note, both the MAPIR cameras had high shutter speeds, but the time to write to the SD card depended on the quality of MicroSD card used. In this case, a U3 rated MicroSD card was used, which yielded a write time of 3 seconds. The thermal camera could be triggered as fast as 1 second.

The flights lasted between 3 and 5 minutes depending upon the wind speed and how many corrections the UAV had to make during the flight. The average flight speed was set at 2 m/s. Immediately after take-off, the temperature of the black thermal target was taken with an infrared thermometer. After each flight, the cameras were turned off, and the data flash and telemetry logs were saved to a laptop used for a ground control station. Due to travel limitations and environmental conditions, all test flights were taken

between 9am and 1pm on data collection days. Due to the start-up procedures of the cameras, each camera was triggered at slightly different locations.

The data from each flight was three sets of data and a single set of GPS coordinates. As noted in the literature review, the cameras were chosen based on their different capabilities in evaluating plant stress, yield, and other properties. The data collected can be used in further studies, however this study focused only on the RGB sensor.

5.3 Image Geolocation and Orthomosaic Creation

The images collected in each flight contained no GPS information. While the MAPIR Survey3 camera had an external GPS which could be mounted, this was not used to create the following workflow to work across all camera types.

Geolocation was first performed. Geolocation is a process where the images were aligned with their GPS coordinates based on the time that the images were captured. Firstly, the GPS tracks was separated into individual flight paths. These flight paths contained dated GPS information of latitude, longitude, altitude, as well as heading. Figure 36 shows an example of the time-stamped data in the GPS Track Editor application presented in chapter 3 (time stamps are in UTC).

Points

S..	#	Date/time	Leg le...	Speed ...	Hea...	Coordinates
	1	9/17/2021 4:22:24 AM	0.0	0.0	0°	35.148378°, -98.
	2	9/17/2021 4:22:25 AM	0.1	0.5	39°	35.148379°, -98.
	3	9/17/2021 4:22:26 AM	0.0	0.0	0°	35.148379°, -98.
	4	9/17/2021 4:22:28 AM	0.0	0.0	0°	35.148379°, -98.
	5	9/17/2021 4:22:29 AM	0.0	0.0	0°	35.148379°, -98.
	6	9/17/2021 4:22:30 AM	0.0	0.0	0°	35.148379°, -98.
	7	9/17/2021 4:22:31 AM	0.0	0.0	0°	35.148379°, -98.
	8	9/17/2021 4:22:32 AM	0.1	0.4	0°	35.148380°, -98.
	9	9/17/2021 4:22:33 AM	0.0	0.0	0°	35.148380°, -98.
	10	9/17/2021 4:22:34 AM	0.0	0.0	0°	35.148380°, -98.
	11	9/17/2021 4:22:35 AM	0.1	0.4	180°	35.148379°, -98.
	12	9/17/2021 4:22:36 AM	0.0	0.0	0°	35.148379°, -98.
	13	9/17/2021 4:22:37 AM	0.1	0.3	270°	35.148379°, -98.
	14	9/17/2021 4:22:38 AM	0.1	0.3	90°	35.148379°, -98.
	15	9/17/2021 4:22:39 AM	0.0	0.0	0°	35.148379°, -98.
	16	9/17/2021 4:22:40 AM	0.0	0.0	0°	35.148379°, -98.
	17	9/17/2021 4:22:41 AM	0.0	0.0	0°	35.148379°, -98.
	18	9/17/2021 4:22:42 AM	0.1	0.4	0°	35.148380°, -98.
	19	9/17/2021 4:22:43 AM	0.1	0.4	0°	35.148381°, -98.
	20	9/17/2021 4:22:44 AM	0.0	0.0	0°	35.148381°, -98.
	21	9/17/2021 4:22:45 AM	0.1	0.4	0°	35.148382°, -98.
	22	9/17/2021 4:22:46 AM	0.0	0.0	0°	35.148382°, -98.
	23	9/17/2021 4:22:47 AM	0.1	0.3	270°	35.148382°, -98.
	24	9/17/2021 4:22:48 AM	0.0	0.0	0°	35.148382°, -98.
	25	9/17/2021 4:22:49 AM	0.1	0.3	90°	35.148382°, -98.
	26	9/17/2021 4:22:50 AM	0.0	0.0	0°	35.148382°, -98.

Figure 36. An example of the time-stamped GPS coordinates

The cameras also provided timestamps for all the images. The two timestamps were then aligned. The application used for aligning images to the GPS coordinates captured during flights was Geosetter, which provided a suite of tools to align multiple images in a batch to the GPS tracks. To find the time offset between images and the GPS data, a single image at a known point was needed. In this case, the point chosen was the first 90 degree turn after waypoint 5 in each flight. Figure 37 shows the image prior to a turn and Figure 38 shows the image captured immediately after.

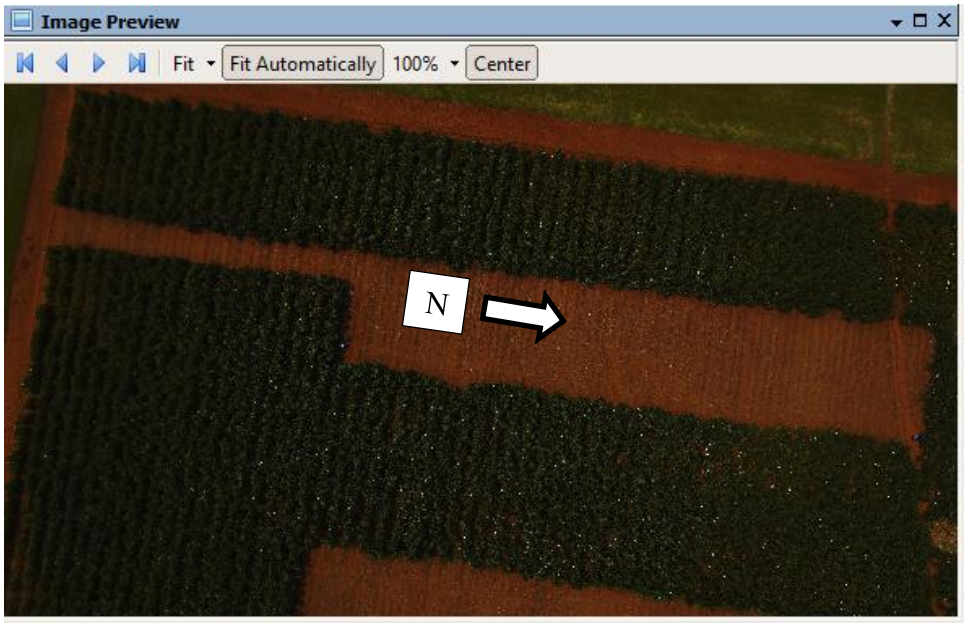

Figure 37. Image preceding turn at the waypoint 5

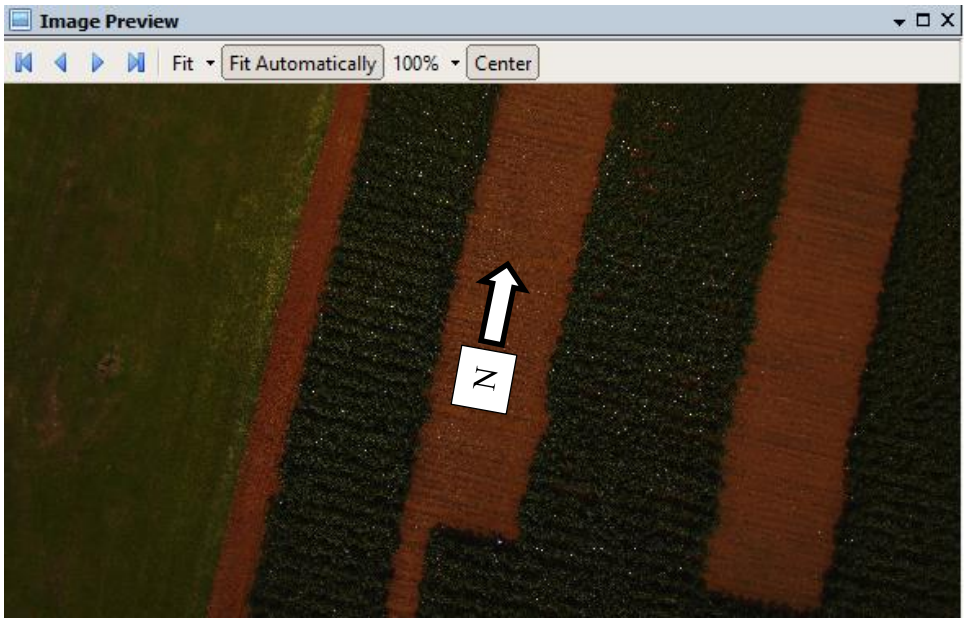

Figure 38. Image following turn at waypoint 5

Using Figure 37 as a reference point, the GPS point which most nearly matched this image could be identified. As mentioned, the first turn is used. Using GeoSetter, the correct point was easy to locate.

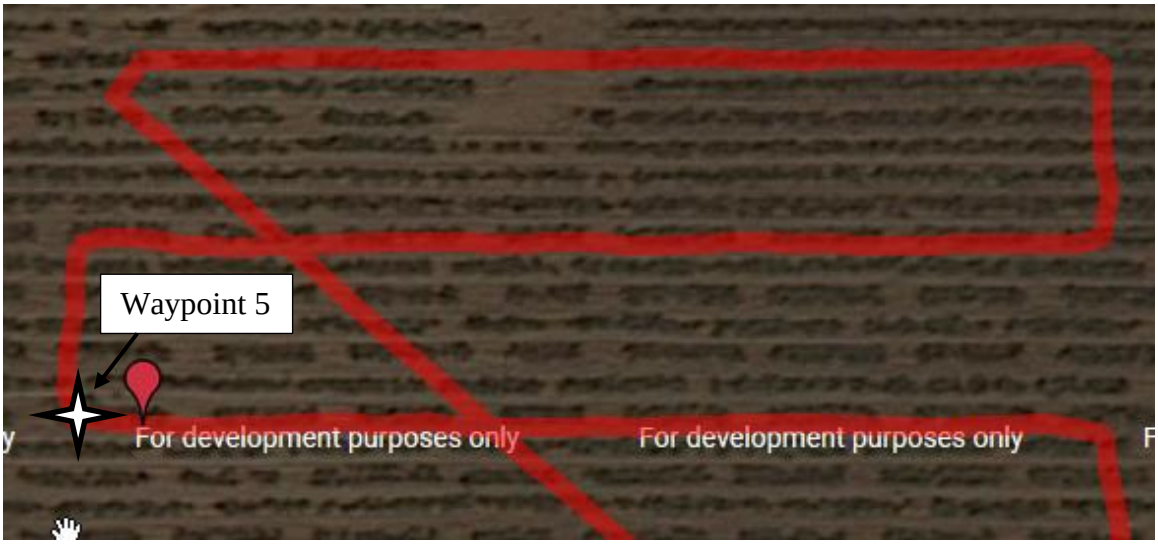

Figure 39. GPS Point prior to Waypoint 5

Figure 40. GPS Point at Waypoint 5

Figure 39 shows the closest GPS point to the waypoint 5 and was matched with the image from Figure 40. GeoSetter then calculated the offsets for all images in a batch.

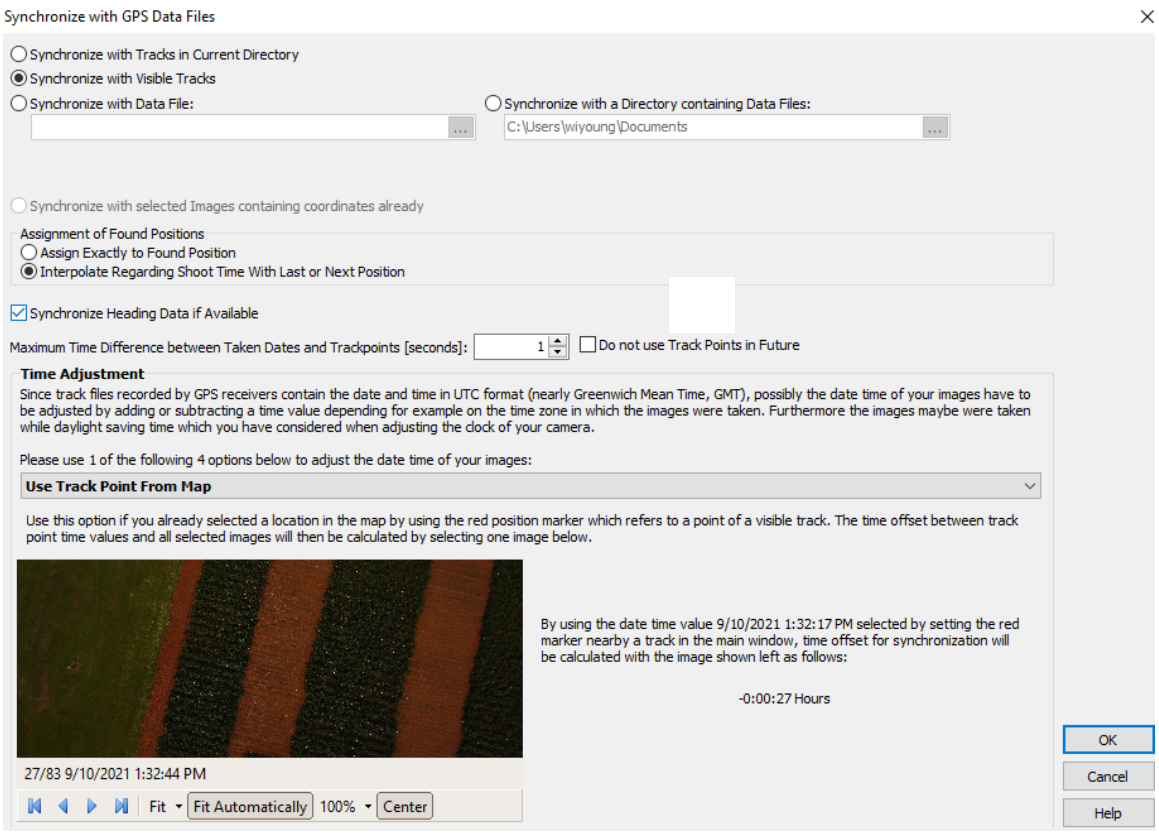

Figure 41. GeoSetter Tools for aligning images to GPS Points

From Figure 41, it could be seen that the time offset between the GPS waypoint from Figure 40 and the image from Figure 38 was 27 seconds. Geosetter then applied this time offset to all the images and interpolated between the GPS points to find the closest point to each image. Each of the marks in Figure 42 shows an image with an aligned GPS location. These images could be used to create an orthomosaic.

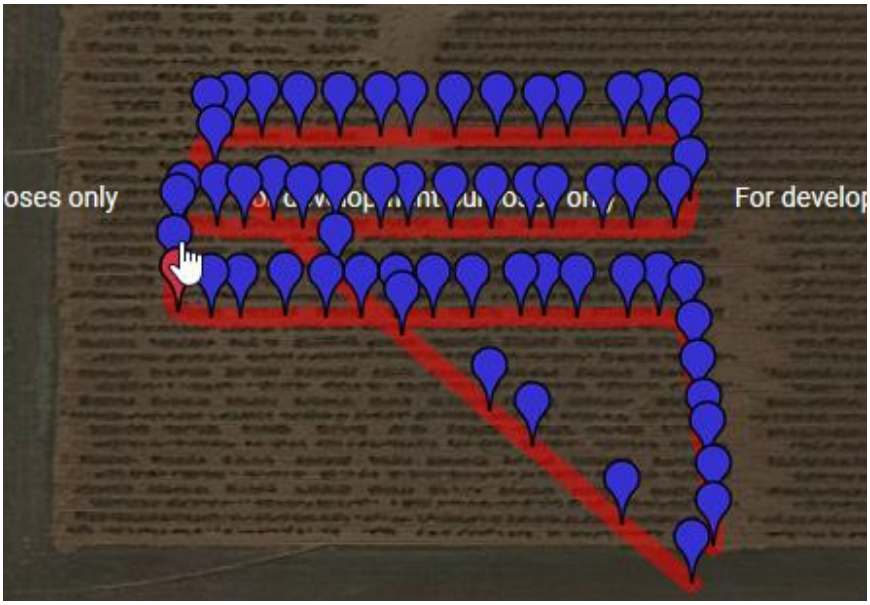

Figure 42. GPS Locations of all images collected from the flight

To create the orthomosaics, WebODM was used. WebODM is based on Open Drone Map, an open-source community driven project to create orthomosaic images. The original Open Drone Map was command line based, whereas WebODM provided a browser-based GUI for easier usage. In general, image stitching software relied on a large amount of memory to function well. Minimum requirements for the program as listed by the Open Drone Map documentation was 16GB of RAM, and 100GB of available storage. A custom-built PC was used in the creation of orthomosaics in this project, with a 128gb of memory, and 2TB of available storage. The computer also has a 12 core, 3.8 GHz AMD Ryzen 9 3900 processor using Ubuntu 20.04 operating system

WebODM uses different methods of image stitching. In this study, the high-resolution option was selected. After selecting the images, WebODM created an orthophoto without further input. The result was an image which opened in WebODM's online map (Figure 43).

Figure 43. Finished Orthophoto in WebODM online viewer

Orthomosaics could then be exported with various projection planes in a .tiff file format. In this case, UTM Zone 14N was used (EPSG:32614). The projection was important to note for exporting the images and importing them into GIS software. In total, 11 orthomosaics were created from the 12 flights, as the contrast on the 30.48m flight on the date of 9-30-2021 was far too low to allow for a quality image to be created.

Each orthomosaic might have a different ground resolution due to the image processing techniques used to match the images together. Table 9 shows the number of images making up each orthomosiac, as well as processing time and ground resolution.

Table 9. Orthomosaic Information

Altitude (m)/(ft)	Date	Number of Images	Processing Time	Average Ground Resolution (cm/px)
30.68/100	9-10	46	5:11	2.66
30.68/100	9-17	46	5:19	2.5
30.68/100	9-23	43	4:54	2.56
30.68/100	9-30	46	5:04	2.82
30.68/100	10-7	56	4:45	2.9
30.68/100	10-14	43	4:36	2.62
60.96/200	9-10	33	4:59	5.29
60.96/200	9-17	34	6:07	5.55
60.96/200	9-23	29	4:51	5.15
60.96/200	9-30	x	x	x
60.96/200	10-7	30	4:36	4.85
60.96/200	10-14	33	7:43	5.43

The theoretical ground resolution for the 30.68m/100ft flights was ~1.4 cm/pixel and 2.806 cm/pixel for the 60.96/200ft flights. As WebODM reported the average ground resolution for each image, it could be noted that there was a loss of resolution when creating orthomosaics.

5.4 Image Alignment in GIS Software and Plot Extraction

QGIS is free and open-source software. Many external plugins were available and could be added into QGIS. In this case study, the “Freehand raster georeferencer”

was installed and used. This tool allowed a user to align multiple geo-tiff images qualitatively, using features from the images. It was important to note that while there were methods to reference the orthomosaics in WebODM directly, it required a different experimental layout including five ground targets of a known location. A qualitative alignment was allowable because of the experimental layout of the crop. In large fields where there were no distinguishing features between plots, ground targets should be used.

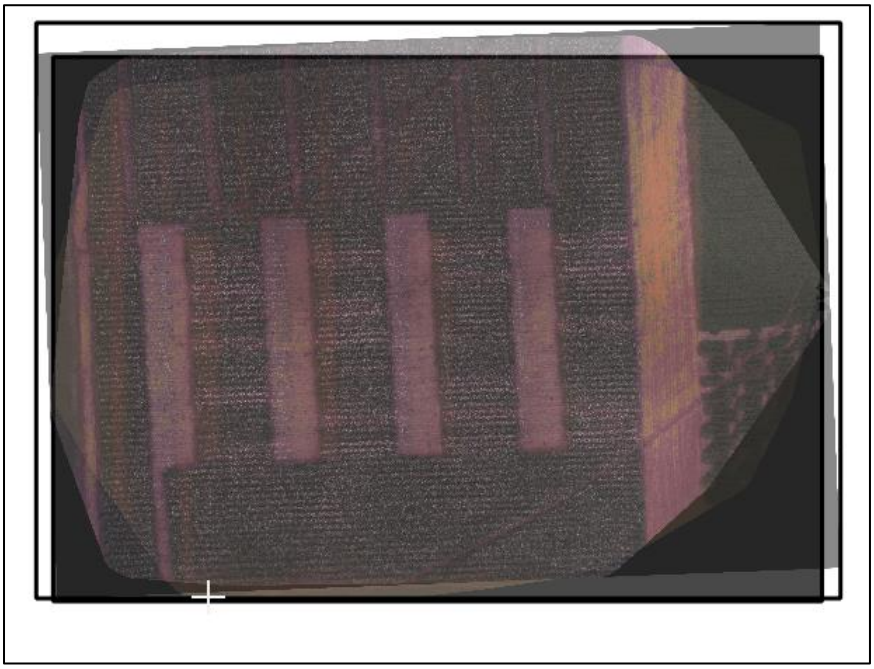

Figure 44. Mis-aligned geo-tiff images

Figure 44 was an example of an obviously misaligned image which could be observed between the rows. Using the QGIS plugin, the images could be stretched and rotated in the same projection plane to align the image of one layer to another (Figure 45).

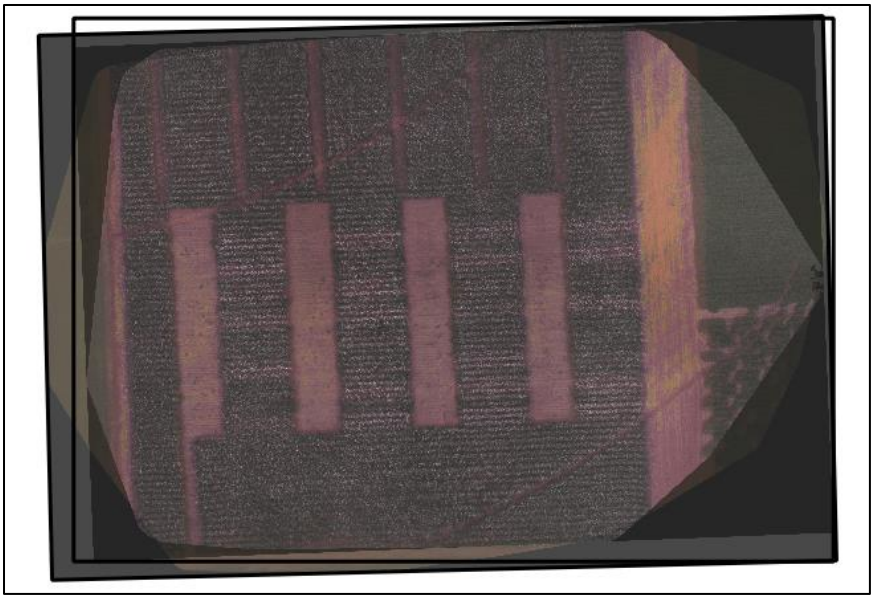

Figure 45. Aligned geo-tiff images

After the alignment, both the images were stacked evenly on top of one another. This process was completed for all images at both flight heights so that all plots were referenced relative to the same location. The positions were not absolute and would not correlate well to actual GPS coordinates of plot locations. This process was completed for all the images across all dates, using the first image (9-10 at 30.48m) as a reference for all other images.

QGIS also had functionality to create shapefiles, and crop raster images (formerly referred to as geo-tiffs) in batch processes. Using this functionality, individual plots could be identified and extracted across all dates.

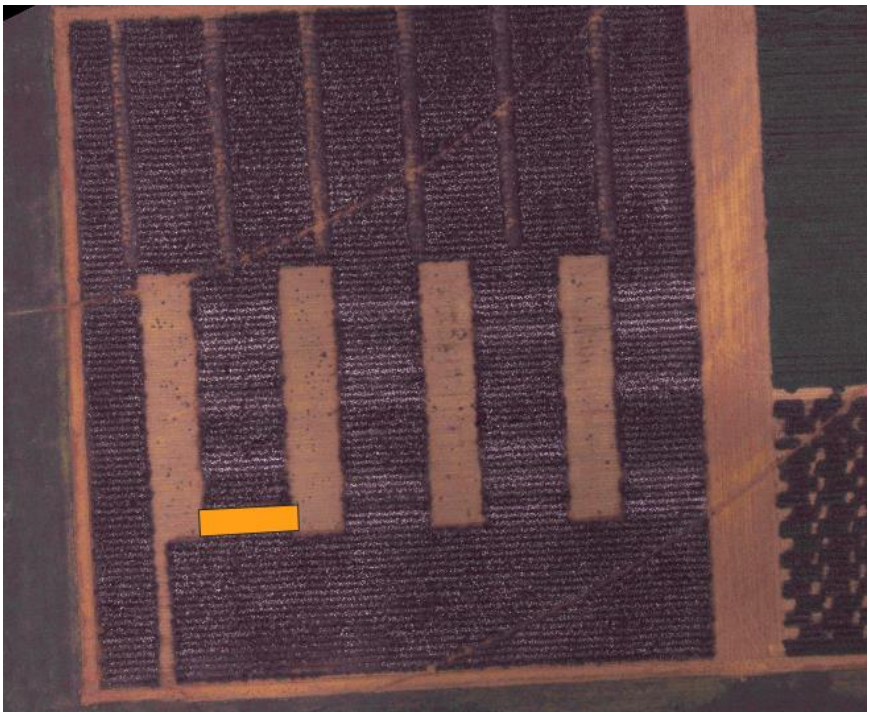

Figure 46. Extracting an individual plots from Raster images

In Figure 46, an individual plot was identified via a shapefile. This shapefile was then used as a cropping extent using QGIS built in “Clip Raster by Extent” function. The results are shown in Figure 47.

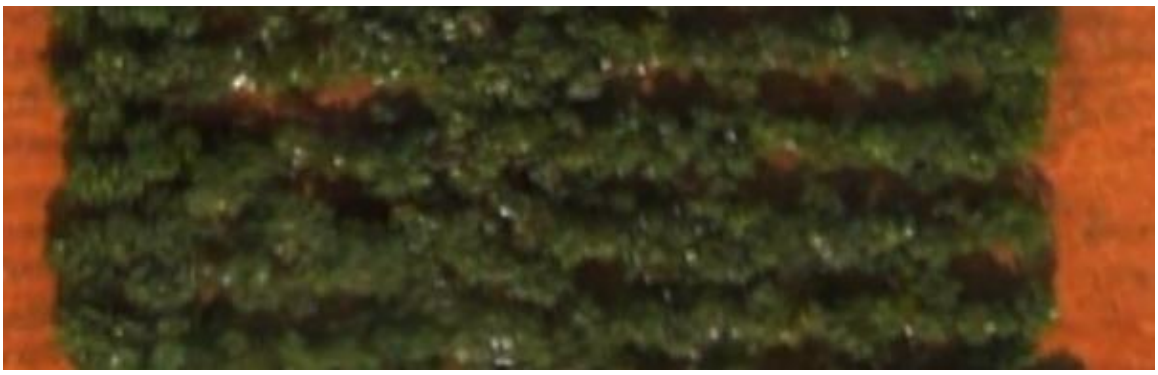

Figure 47. Clipped Raster Image

The extracted plots were able to go through additional post-processing techniques for data analysis. Different programming languages and analysis could be used. In this

case study, a Python program was developed to calculate the number of cotton pixels in the image vs the number of pixels which were not identified as cotton. Simple manual thresholding was used to complete the analysis using OpenCV Python library.

5.5 Image Analysis

To stay within the scope of this thesis, a single plot was extracted across all dates. While the remaining data could be used in future analysis. A single plot across all dates served as a demonstration that processing the data captured by the developed UAV platform could be done at no cost outside of hardware. Figure 48 shows a flowchart of data processing algorithm for cotton maturity rating.

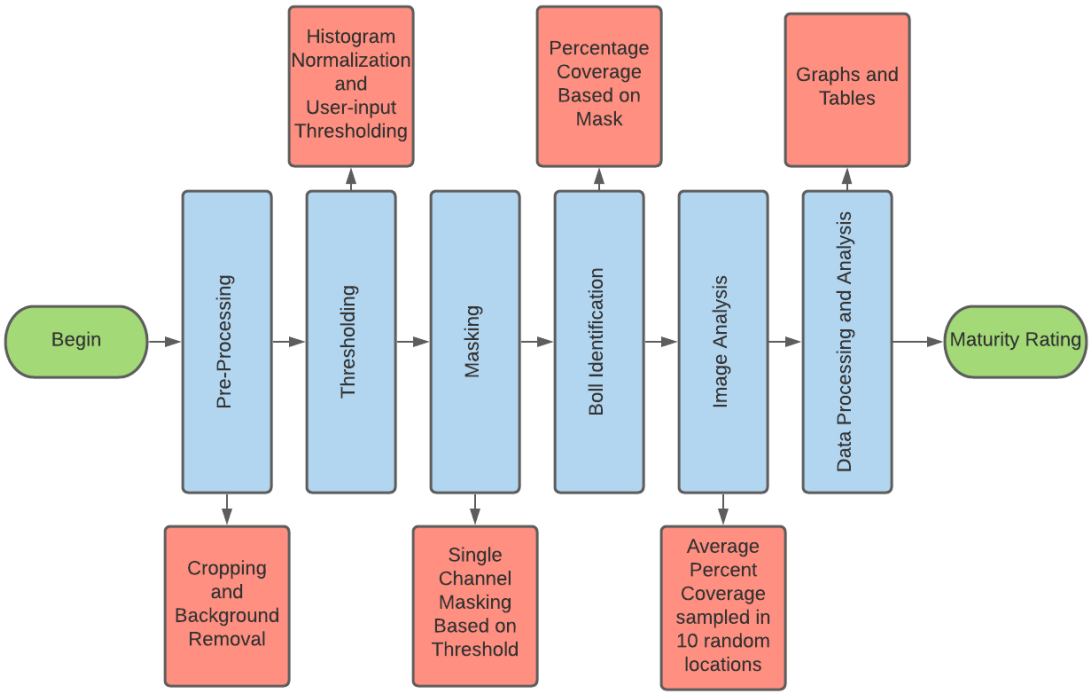

Figure 48. Cotton Maturity Rating Algorithm

After image normalization, a histogram of the image was generated (Figure 49) and the first low frequency asymptote of the histogram was identified. The second mode

of the histogram showed the region where cotton bolls and bright white soil backgrounds could be observed. Using this location as a threshold, a binary mask was created and used for further analysis (Figure 50).

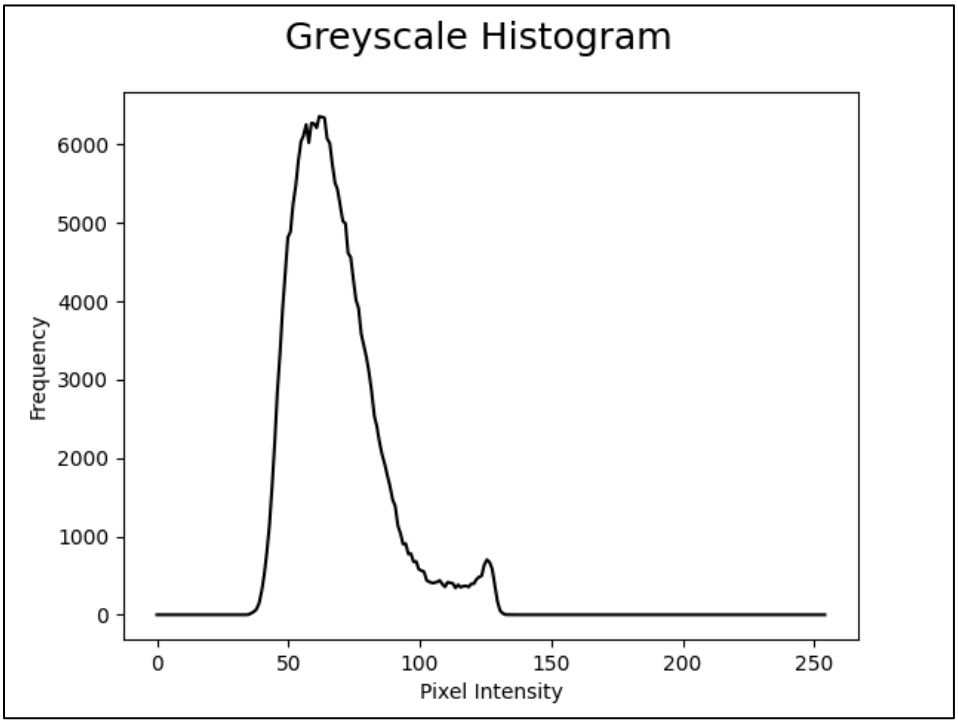

Figure 49. Bimodal Histogram of Cotton Plot

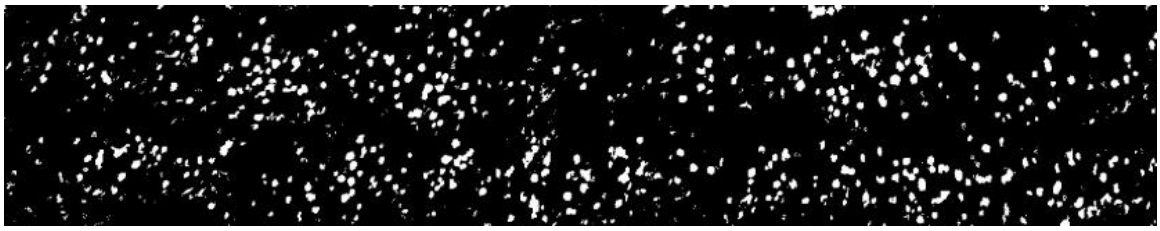

Figure 50. A image mask showing cotton bolls

After the image mask was created (Figure 50), the data could be correlated with the manual, ground-truth ratings of an agronomist. As there was insufficient data to show a true correlation, and further analysis will be left to future studies. To gather quantitative data from the image mask, 10 random 100pixel × 100pixel areas were identified on each

plot. The percent image coverage (white vs black pixels) was calculated, and then averaged across all 10 samples.

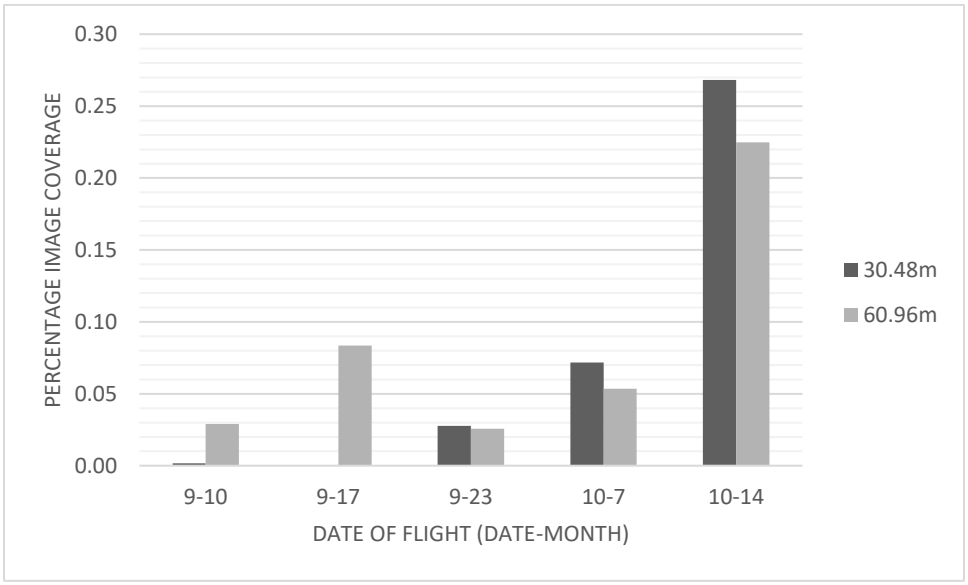

Figure 51. Percent Image Coverage

Figure 51 shows the percent image coverage of each plot extracted in section 6.4. Between the dated of 10-7 and 10-14, harvest aids were applied to the crop, which resulted in a greater amount of visible cotton. On the date of 9-17, the 30.48m altitude flight yielded data which was unsuitable for analysis. The higher relative value on the date of 9-17-2021 for 60.96m altitude might be due to capturing more of the soil background than anticipated. This algorithm should be used multiple times to verify there was no selector bias as well.

5.6 Summary

The case study presented an example workflow for using image captured by the developed UAV platform without any GPS coordinates and creating useable data from the images. Methods for geo-locating images with Geosetter proved to work and were a simple solution for all images on different dates. Free-to-use WebODM provided a

simple browser-based interface and resulted in ground resolutions roughly half of what was theoretically possible. QGIS and plot extraction allowed for individual plots to be extracted and cropped into their own individual files. Throughout most of the process, batch methods were able to be used to lighten the user's workload. None of the programs used were paid programs, and all of them will run on basic Windows desktop workstation (aside from WebODM, which used a custom-built computer for higher memory amounts). The study showed that the images collected by the UAV platform could be processed from this custom-built platform without any additional complications or costs.

CHAPTER VI

CONCLUSIONS

The purpose of this thesis was to construct a UAV for use in small research plots. The UAV was designed and constructed from off-the-shelf and readily available components, using a Cube Orange flight controller. A HERE3 GNSS GPS unit was used and had RTK functionality. In a series of experiments, the average lateral error of the UAV was 0.2m at an altitude of 30.48m, and 0.22m at an altitude of 60.96m. Lateral error was defined as the variance of the UAV's actual flight path from the planned flight path. Altitude error according to EKF was 0.06m, while the built-in barometer gave an average of 0.33m. There was no significant difference in average errors between the two flight heights. Battery life was found to be an average of 8 minutes per flight with a 700 gram payload. Average battery usage was 0.244 volts/minute in average wind conditions in Southwest Oklahoma.

A two axis pan-tilt servo gimbal was also designed and constructed to keep the cameras facing in a downward direction. This gimbal was capable of carrying up to three different cameras in several orientations. With three cameras affixed to the gimbal, the maximum average instantaneous error in pitch and roll was 1.2 degrees and 1.7 degrees, respectively. The effects of mounting cameras in an off-centered method led to higher

errors. As this UAV captured only still images and not videos, the relatively small errors are allowable.

A case study was performed over a cotton maturity timing trial to validate the system and demonstrate the image processing pipeline. Through the uses of several different programs, a data set of orthomosaic images were created from images captured by the UAV platform. GIS systems were then used to align the images between dates and extract plots, and a Python script was used to perform image analysis relating to the visible cotton bolls in each image.

There were challenges associated with quality image alignment and georeferencing. With the ease of use of modern electronics and GPS systems, further research should be conducted to find a way to embed GPS data in the metadata of images collected with this UAV. Embedded GPS data will increase the ease of use for the UAV and eliminate 3 steps in the image processing pipeline. Figure 52 shows the completed platform.

Figure 52. Completed UAV platform

5.2 Contribution to Knowledge

The system is robust, simple to use, and utilizes free software. This study demonstrates that UAVs related research may not need to be cost prohibitive, and users may not need a strong knowledge of embedded electronics or programming to effectively use the system. This system should provide researchers with the ability to quickly and efficiently construct a platform to collect data, without extraordinary expenses related to off the shelf components. The configurability of the platform should allow anyone to optimize for their specific research needs.

REFERENCES

Barry, P., & Coakley, R. (n.d.). *Accuracy of UAV Photogrammery Compared with Network RTK GPS*. Retrieved November 2, 2021, from http://uav.ie/PDF/Accuracy_UAV_compare_RTK_GPS.pdf

Billingsley, J., Visala, A., & Dunn, M. (1984). Robotics in A. *Real-time computer control, ed. Bernett S., Linkens DA, lEE Control Engineering Series, 24*, 216-226.

Boman, R. (2015). Cotton crop maturity determination - extension.okstate.edu. Retrieved October 19, 2021, from https://extension.okstate.edu/programs/cotton/site-files/docs/crop_maturity_determination_handout_final_2015.pdf

Byrd, S. (2019, September 01). 2019 Oklahoma Cotton Harvest Aid Guide - Oklahoma State University. Retrieved October 19, 2021, from https://extension.okstate.edu/fact-sheets/2019-oklahoma-cotton-harvest-aid-guide.html

Chen, T., Yang, W., Zhang, H., Zhu, B., Zeng, R., Wang, X., . . . Zhang, L. (2020). Early detection of bacterial wilt in peanut plants through leaf-level hyperspectral and unmanned aerial vehicle data. *Computers and Electronics in Agriculture, 177*, 105708.

Deng, L., Mao, Z., Li, X., Hu, Z., Duan, F., & Yan, Y. (2018). UAV-based multispectral remote sensing for precision agriculture: A comparison between different cameras. *ISPRS Journal of Photogrammetry and Remote Sensing, 146*, 124-136.

Feng, A., Zhou, J., Vories, E. D., Sudduth, K. A., & Zhang, M. (2020). Yield estimation in cotton using UAV-based multi-sensor imagery. *Biosystems Engineering, 193*, 101-114.

Freeman, P. K., & Freeland, R. S. (2015). Agricultural UAVs in the U.S.: potential, policy, and hype. *Remote Sensing Applications: Society and Environment, 2*, 35-43. doi:https://doi.org/10.1016/j.rsase.2015.10.002

Geosetter, 2022. https://geosetter.de/en/donation-en/. Accessed September 2021.

Herwitz, S. R., Johnson, L. F., Dunagan, S. E., Higgins, R. G., Sullivan, D. V., Zheng, J., Brass, J. A. (2004). Imaging from an unmanned aerial vehicle: agricultural surveillance and decision support. *Computers and Electronics in Agriculture, 44*(1), 49-61.

Jay, S., Comar, A., Benicio, R., Beauvois, J., Dutartre, D., Daubige, G., Baret, F. (2020). Scoring Cercospora Leaf Spot on Sugar Beet: Comparison of UGV and UAV Phenotyping Systems. *Plant Phenomics, 2020*, 9452123.

JérômeThéau, ErwanGavelle, & PatrickMénard. (2020). Crop scouting using UAV imagery: a case study for potatoes. *Journal of Unmanned Vehicle Systems, 8*(2), 99-118.

Keane, J. F., & Carr, S. S. (2013). A brief history of early unmanned aircraft. *Johns Hopkins APL Technical Digest, 32*(3), 558-571.

Kerkech, M., Hafiane, A., & Canals, R. (2020). Vine disease detection in UAV multispectral images using optimized image registration and deep learning segmentation approach. *Computers and Electronics in Agriculture, 174*, 105446.

Li, L., Fan, Y., Huang, X., & Tian, L. (2016). *Real- time UAV weed scout for selective weed control by adaptive robust control and machine learning algorithm*. Paper presented at the 2016 ASABE Annual International Meeting, St. Joseph, MI.

Matese, A., Toscano, P., Di Gennaro, S. F., Genesio, L., Vaccari, F. P., Primicerio, J., . . . Gioli, B. (2015). Intercomparison of UAV, Aircraft and Satellite Remote Sensing Platforms for Precision Viticulture. *Remote Sensing, 7*(3), 2971-2990.

Messina, G., & Modica, G. (2020). Applications of UAV Thermal Imagery in Precision Agriculture: State of the Art and Future Research Outlook. *Remote Sensing, 12*(9), 1491.

Niemiec, R., Gandhi, F., & Singh, R. (2018). Control and Performance of a Reconfigurable Multicopter. *Journal of Aircraft, 55*(5), 1855-1866.

Schimmelpfennig, D. (2016). *Farm Profits and Adoption of Precision Agriculture*. Retrieved from https://ageconsearch.umn.edu/record/249773/files/err-217.pdf

Stotts, D. (2021). General settings registry. Retrieved October 19, 2021, from http://www.dasnr.okstate.edu/Members/donald-stotts-40okstate.edu/oklahoma-moves-up-in-national-rankings-as-cotton-producer

Theys, B., Dimitriadis, G., Hendrick, P., & Schutter, J. D. (2016) *Influence of propeller configuration on propulsion system efficiency of multi-rotor Unmanned Aerial Vehicles.* Paper presented at the 2016 International Conference on Unmanned Aircraft Systems (ICUAS), 2016, 7-10 June 2016.

Tsouros, D. C., Bibi, S., & Sarigiannidis, P. G. (2019). A Review on UAV-Based Applications for Precision Agriculture. *Information, 10*(11), 349.

Wójtowicz, M., Wójtowicz, A., & Piekarczyk, J. (2016). Application of remote sensing methods in agriculture. *Communications in Biometry and Crop Science, 11*(1), 31-50.

Yang, C., Westbrook, J. K., Suh, C. P.-C., Martin, D. E., Hoffmann, W. C., Lan, Y., Goolsby, J. A. (2014). An Airborne Multispectral Imaging System Based on Two Consumer-Grade Cameras for Agricultural Remote Sensing. *Remote Sensing, 6*(6), 5257-5278.

Zhang, C., Marzougui, A., & Sankaran, S. (2020). High-resolution satellite imagery applications in crop phenotyping: An overview. *Computers and Electronics in Agriculture, 175*, 105584.

Zhou, J., Zhou, J., Ye, H., Ali, M. L., Nguyen, H. T., & Chen, P. (2020). Classification of soybean leaf wilting due to drought stress using UAV-based imagery. *Computers and Electronics in Agriculture, 175*, 105576.

VITA

William Wade Young

Candidate for the Degree of

Master of Science

Thesis: DEVELOPMENT OF AN UNMANNED AERIAL VEHICLE AND IMAGE PROCESSING TECHNIQUES FOR AGRICULTURAL APPLICATIONS

Major Field: Biosystems Engineering

Biographical:

Education:

Completed the requirements for the Master of Science in Biosystems Engineering at Oklahoma State University, Stillwater, Oklahoma in May, 2022.

Completed the requirements for the Bachelor of Science in Biosystems Engineering at Oklahoma State University, Stillwater, Oklahoma in 2020.

Experience:

Graduate Research Assistant, June 2020-May 2022

Undergraduate Research Assistant September 2019- June 2020

Professional Memberships:

American Society of Agricultural and Biological Engineers